

Complex molecule formation in grain mantles

P. Hall^{1,2} and T. J. Millar³

¹ Department of Physics, UMIST, P.O. Box 88, Manchester, M60 1QD, UK.

² Astronomy Department, Cornell University, Ithaca, New York, 14853-6801, USA.

³ Astrophysics Research Centre, School of Mathematics and Physics, Queen's University, Belfast, BT7 1NN, Northern Ireland.

Preprint online version : 31 March 2010

ABSTRACT

Context. Complex molecules such as ethanol and dimethyl ether have been observed in a number of hot molecular cores and hot corinos. Attempts to model the molecular formation process using gas phase only models have so far been unsuccessful.

Aims. To demonstrate that grain surface processing is a viable mechanism for complex molecule formation in these environments.

Methods. A variable environment parameter computer model has been constructed which includes both gas and surface chemistry. This is used to investigate a variety of cloud collapse scenarios.

Results. Comparison between model results and observation shows that by combining grain surface processing with gas phase chemistry complex molecules can be produced in observed abundances in a number of core and corino scenarios. Differences in abundances are due to the initial atomic and molecular composition of the core/corino and varying collapse timescales.

Conclusions. Grain surface processing, combined with variation of physical conditions, can be regarded as a viable method for the formation of complex molecules in the environment found in the vicinity of a hot core/corino and produce abundances comparable to those observed.

Key words. Stars: formation. ISM: molecules – abundances

1. Introduction

A number of complex molecules have been discovered in the interstellar medium. First was methanol, CH₃OH, (Ball 1970) followed by dimethyl ether, CH₃OCH₃, (Snyder et al. 1974) and ethanol, CH₃CH₂OH, (herein denoted C₂H₅OH) (Zuckerman et al. 1975). A variety of other isomers, isotopic variants and similar compounds have also been seen. Charnley et al. (1995) review the distribution of complex molecules while Ikeda et al. (2001 & 2002) present more recent observations. CH₃OH is seen in cold dark clouds with a relative abundance of 10⁻⁹ (with respect to H₂) while in hot cores this can be as large as 10⁻⁶. The highest abundances are observed in regions where grain mantles are likely to have recently evaporated, strongly suggesting mantle processing either directly or in the formation of precursors.

A variety of computer models have been constructed to investigate molecule formation. Predominantly these are based on chemical reaction networks and use a “flat” (fixed) parameter space. As with the models presented here most are “single point”, where a single representative point in a cloud is modelled. This is satisfactory as chemistry at another point with different physical parameters could be modelled simply by changing the parameters. Over time the size and complexity of the reaction networks has increased as more reaction rate data is published in the literature and greater computer power becomes available to process more complex networks. (See Millar (1990) for a review of model development.) Millar et al. (1991b) model the production of CH₃OH by a fixed parameter gas-phase-only model and are unable to produce abundances in excess of 10⁻⁷ lending further weight to the involvement of grain mantle processing. C₂H₅OH is seen in fewer sources than CH₃OH and

all known sources are dense, hot core star-forming regions, exactly the places where grain mantles are likely to evaporate. Abundances are in the range 10⁻⁹-10⁻⁸ (with respect to H₂). CH₃OCH₃ is often seen in the same sources as C₂H₅OH and has recently been detected in hot corinos (Ceccarelli et al. 2004; Bottinelli et al. 2004). It has an abundance range of 10⁻⁸-10⁻⁶ and the CH₃OCH₃/C₂H₅OH abundance ratio differs greatly between apparently similar sources. (Abundances with respect to H₂ for selected sources are listed in Table 1.)

Table 1. Observed fractional abundances of complex molecules

Source - Hot Core	CH ₃ OH	C ₂ H ₅ OH	CH ₃ OCH ₃
NGC6334F	2.0 × 10 ⁻⁷	9.0 × 10 ⁻⁹	4.0 × 10 ⁻⁸
G327.3-0.6	1.0 × 10 ⁻⁷	1.0 × 10 ⁻⁸	3.0 × 10 ⁻⁸
G31.41+0.31	9.0 × 10 ⁻⁸	2.0 × 10 ⁻⁸	2.0 × 10 ⁻⁸
G34.3+0.2	9.0 × 10 ⁻⁸	6.0 × 10 ⁻⁹	1.0 × 10 ⁻⁸
G10.47+0.03	2.0 × 10 ⁻⁷	1.0 × 10 ⁻⁸	3.0 × 10 ⁻⁸
Sgr B2 (N)	2.0 × 10 ⁻⁸	1.0 × 10 ⁻⁹	7.0 × 10 ⁻¹⁰
DR21(OH)	1.0 × 10 ⁻⁸		
W3(H ₂ O)	4.0 × 10 ⁻⁸		
W51 e1/e2	3.0 × 10 ⁻⁷	9.0 × 10 ⁻⁹	
Orion Compact Ridge	2.0 × 10 ⁻⁷		
Orion Hot Core	1.0 × 10 ⁻⁶	2.0 × 10 ⁻⁸	
Source - Hot Corino			
IRAS16293-2422	1.0 × 10 ⁻⁷		2.4 × 10 ⁻⁷
NGC1333-IRAS4A	< 1.0 × 10 ⁻⁸		< 2.8 × 10 ⁻⁸
NGC1333-IRAS4B	7.0 × 10 ⁻⁷		< 1.2 × 10 ⁻⁶
NGC1333-IRAS2A	3.0 × 10 ⁻⁷		3.0 × 10 ⁻⁸

Data from Ikeda et al. 2001; Ikeda et al. 2002; Bottinelli et al. 2007

Send offprint requests to: P. Hall

e-mail: phall@isc.astro.cornell.edu

Even under very favorable conditions fixed parameter gas-phase-only chemical models produce maximum abundances for $\text{C}_2\text{H}_5\text{OH}$ and CH_3OCH_3 of the order of 10^{-11} (Herbst & Leung 1989; Millar et al. 1991a; Charnley et al. 1992), between two and five orders of magnitude below that observed. Again this suggests a scenario in which mantles form on dust grains at some point in a cloud's lifetime when conditions are favorable. The mantles are active and complex molecules (or their precursors) form on them more efficiently than in the gas phase. Later the cloud evolves becoming warmer and denser and the contents of the mantles pass back into the gas phase. Several other gas-phase-only models (for example Charnley et al. 1992; Caselli et al. 1993) have demonstrated that the chemistry in hot cores is active, with particular gas phase reaction channels initiated with simple species thought to originate from mantles, a possible explanation for observed complex molecule abundances.

A number of more in-depth models have included surface reaction chemistry. One of the first has been developed by Hasegawa et al. (1992) and Hasegawa & Herbst (1993). This model has 274 chemical species with 2928 reactions and includes 1% (by mass) dust grains in the gas cloud. Molecules can freeze out onto grains and later pass back into the gas phase. Once on a grain heavier species molecules are held stationary at lattice binding sites while lighter species, most commonly hydrogen atoms, can migrate around the grain. When mobile light species encounter fixed heavy species the two can combine to produce progressively larger molecules. While large molecules can thaw off the grain surface there are a number of other possible desorption mechanisms that can act as well. (See Section 2.3.) One additional benefit of this approach is that grain surface catalysis of hydrogen molecules can be modelled directly.

Shalabiea & Greenberg (1995) then take the next logical step in interstellar cloud modelling by including variations in physical parameters. They use a gas phase reaction rate network and interchange between gas and surface similar to Hasegawa et al. (1992) and Hasegawa & Herbst (1993). However certain physical parameters (eg. density) can also change. Shalabiea & Greenberg (1995) model these by including differential equations for them and solving for the relevant parameter(s) at each point in time in much the same way as species abundances are solved for. They also coin the terms “pseudo-time-dependent”, where the model chemistry evolves over time while the parameters are static and “real-time-dependent” where both chemistry and physical parameters evolve. Their paper provides comparison between the two types, with the gas and grain model including 218 chemical species and 2075 reactions. With the more recent identification of “hot corinos” (Table 1 & Section 3.1) where the temperature range is optimal for the grain surface production of larger molecules and their subsequent return to the gas phase some specific modelling of these type of objects has been done. Garrod & Herbst (2006) use a gas and grain reaction network with 655 species and 6509 reactions. The same model was used by Aikawa et al. (2008). Subsequently Garrod et al. (2008) produced an extended and more generalized version. Comparison of the output of these models with the results presented here is made in Section 5.

As is discussed further in Section 2.3 some mechanism(s) must be returning material from grain mantles back to the gas phase since the alternative is depletion of molecular species heavier than H_2 in a timescale shorter than the lifetime of known clouds, which is not seen. More recent modelling work has focused on the investigating the effectiveness of several proposed desorption mechanisms. Willacy & Millar (1998) provide a set of gas and surface models which include different desorption

mechanisms and compare their effectiveness. These models use 282 species and 4864 reactions. Garrod et al. (2007) specifically model formation of CH_3OH in a quiescent cloud and point out that if grain surface processes are invoked to explain the abundance of CH_3OH then at least one non-thermal desorption mechanism must be active. Tielens & Charnley (1997) have argued that, at least in some cases, the reaction network model cannot be justified and that a Monte Carlo simulation approach is more appropriate. This has led to some debate in the current literature about the relative merits of the two methods. Willacy & Millar (1998) discuss this and conclude that currently there are computational impracticalities in using the Monte Carlo approach in real-time-dependent models, and further that the two different approaches may give fairly similar results for systems of increasing complexity. A direct comparison of the two approaches by Garrod et al. (2009) demonstrates considerable similarity between them. Certainly previous gas phase only reaction rate models have yielded results comparable with observations for many species.

The model used here builds on its predecessors. Termed the “Gas/Surface” model it is a single point, gas and surface phase, chemical reaction network model with 279 species and 2968 reactions. It includes the grain surface mechanism used by Hasegawa et al. (1992) and Hasegawa & Herbst (1993) as well as the desorption mechanisms discussed by Willacy & Millar (1998). It is also fully “real-time-dependent”. Instead of the differential equation approach taken by Shalabiea & Greenberg (1995) each separate time step has its own set of physical parameters which are fed into the model from a storage file at the beginning of each time step. This approach has several advantages. Firstly it reduces computational strain on the model since there is no additional equation solving necessary. This is particularly important in situations where parameters are changing very quickly and there are major differences between adjacent time steps. (For example in the final stages of a cloud collapse where density increases drastically in a short time.) Secondly, this approach allows the same set of software to be used to model multiple different situations with no reprogramming at all. Only the input parameter file has to be changed. This allows great flexibility in the scope of scenarios that could be investigated. Further, in certain situations where there are major, abrupt changes in physical parameters (eg. shocks), the differential equation approach is highly prone to breakdown as generating a numerical solution for a given parameter requires some level of continuity between one time step and the next, whereas the parameter file approach avoids this problem completely.

The Gas/Surface model is used here to investigate the scenario of complex molecule formation in grain mantles and their subsequent release back into the gas phase. We consider clouds at a variety of initial densities with different exposure to photoionization. As these clouds collapse to become denser and darker, their chemistry becomes more complex and their temperature drops allowing grain mantles to form. Simple gas-phase dominated chemistry at the beginning leads to the deposition of a variety of basic molecules onto an initially bare grain surface. Once on the grain, surface processes allow the build up of complex molecules in a frozen mantle. Later, as the cloud heats up, the mantle evaporates introducing the complex molecules into the gas phase with a variety of chemical consequences significantly different from gas phase only processing.

2. The Gas/Surface Model

2.1. Design of the model

The Gas/Surface model is used here to model a collapse situation. A cloud collapse begins with the cloud optically thin and open to heating by external photons. Self shielding of H_2 is treated by the method of Wagenblast (1992). As it contracts it eventually becomes optically thick to external photons and its inner regions cool. It is this cooling which allows molecules to freeze out onto dust grain surfaces and form mantles. Eventually continuing collapse of the cloud, assisted possibly by the ignition of a proto-star at its center, causes the temperature to rise again desorbing the mantles off the grain and returning mantle processed species to the gas phase. The model allows interchange between gas and surface phases, both freezing, thermal desorption and a variety of other continuously acting desorption mechanisms, as described by Willacy (1993) and Willacy & Millar (1998). (See Section 2.3.) Once on the grain surface chemistry takes place as described in Section 2.2.

The reaction networks are solved numerically using the GEAR package (Hindmarsh 1974, 1983). It is the combination of both a time variable parameter space and interchange between gas and surface phase chemistry that makes the Gas/Surface model appropriate to investigate complex molecule formation. A fuller description of the model design can be found in Hall (1997).

2.2. Surface chemistry mechanism

The surface chemistry mechanism used in the Gas/Surface Model is taken from Hasegawa et al. (1992) and Hasegawa & Herbst (1993) with additional complex molecule formation reactions listed in the Appendix. Surface species are prefixed “*” to distinguish them from their gas phase counterparts. This scheme allows fourteen low molecular mass species (Table 2) to be mobile on the grain surface while all other surface species are stationary, held at “sites” on the surface. The adsorption energy E_D (in K) is the energy needed to liberate the species from the grain surface back into the gas phase. Parameter values (and their references) are listed in Table 4.

The mobile species migrate around the grain surface by “hopping” from site to site. A mobile species arriving at an occupied site can react with either a stationary species already there or another mobile species which has also just arrived. Mobile species are regarded as occupying any given site for a finite period of time, generally about 10^{-12} s, the exact time being determined by species mass and prevailing temperature. There is an energy potential barrier separating adjacent sites and mobile species must possess sufficient energy to overcome it. For most of the mobile species “classical” type motions only are permitted. The species must have sufficient classical kinetic energy to cross potential barriers. For atomic and molecular hydrogen however quantum tunnelling through barriers is permitted. Which reactions take place is governed by a reaction set (Section 2.4) analogous to those used for gas phase reactions, each with an accompanying rate coefficient. The grain itself is assumed to be inert and all surface chemistry involves the mantle only. The classical mobile species migrate over the grain surface. The time to move between two adjacent surface sites (“hopping time”) t_{hop} is given by :

$$\frac{1}{t_{hop}} = \nu_0 \exp\left(\frac{-E_b}{kT}\right) \quad (1)$$

Table 2. Mobile surface species

	Species	Adsorption Energy E_D/k (K)	Ref.
1	*H	350.0	1
2	*H ₂	450.0	1
3	*He	100.0	2
4	*C	800.0	1
5	*N	800.0	1
6	*O	800.0	1
7	*S	1100.0	1
8	*CH	645.0	3
9	*NH	604.0	3
10	*OH	1259.0	3
11	*CH ₂	956.0	3
12	*NH ₂	856.0	3
13	*CH ₃	1158.0	3
14	*NH ₃	1107.0	3

References. (1) Tielens & Allamandola 1987; (2) Tielens & Hagen 1982; (3) Allen & Robinson 1977;

where T is the grain surface temperature and E_b is the potential energy barrier between adjacent surface sites, $E_b \approx 0.3E_D$. The parameter ν_0 is the characteristic vibration frequency for the mobile species (assumed isotropic). Its value (in Hz) is given by :

$$\nu_0 = \sqrt{\frac{2n_s E_D}{\pi^2 m}} \quad (2)$$

where n_s is the surface density of sites ($\approx 1.5 \times 10^{19} \text{ m}^{-2}$) and m is the mass of the mobile species (in kg). This gives values of ν_0 in the range 10^{12} - 10^{13} s^{-1} . Hydrogen atoms and molecules are held to be quantum particles and their hopping times are given by the time for them to quantum tunnel through the potential barrier :

$$\frac{1}{t_{hop}} = \nu_0 \exp\left[\frac{-2a}{\hbar} \sqrt{2mE_b}\right] \quad (3)$$

where a is the separation between two adjacent sites ($\approx 10^{-10} \text{ m}$). The diffusion time, t_{diff} , for a mobile species to scan the entire grain surface is given by :

$$t_{diff} = N_s t_{hop} \quad (4)$$

where N_s is the total number of surface sites on a grain ($N_s = 10^6$). The surface reaction rate coefficient k_{ij} between two surface species i and j by classical diffusion is given by :

$$k_{ij} = \frac{\kappa_{ij} \left(\frac{1}{t_i} + \frac{1}{t_j}\right)}{N_s n_g} \quad (5)$$

where t_i and t_j are the hopping times for species i and j and n_g is the number density of grains. A gas:grain ratio of 100:1 by mass, $1:1.33 \times 10^{-12}$ by number is used. The factor κ_{ij} is the reaction probability for a specific reaction. $\kappa_{ij} = 1.0$ unless the associated activation energy (E_a) is non-zero. Non-zero activation energy enables certain reaction channels to be favoured over others. In the classical case :

$$\kappa_{ij} = \exp\left(\frac{-E_a}{kT}\right) \quad (6)$$

In the quantum case where at least one of the reactants is a hydrogen atom or molecule :

$$\kappa_{ij} = \exp \left[\frac{-2a}{\hbar} \sqrt{2\mu E_a} \right] \quad (7)$$

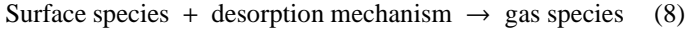
where μ (kg) is the reduced mass in a two-body collision.

2.3. Desorption mechanisms

Desorption mechanisms can be divided into two basic classes, continuously acting which remove a few atoms/molecules at any one time and irregular such as shocks, which occur at random intervals but return most or all of a grain mantle to the gas phase. In the scenarios modelled here there are no shocks or similar mechanisms of sufficient strength to desorb mantles and continuous mechanisms dominate. Willacy (1993) provides an in-depth treatment of continuous mechanisms and four of them have been included in the models presented here :

1. Mantle Explosion
2. Direct UV Photodesorption
3. Cosmic Ray Induced Photodesorption
4. Direct Heating by Cosmic Rays

For each desorption mechanism an equation is provided in the reaction set with its own rate coefficient k :



One of these four mechanisms, direct UV photodesorption, dominates when a cloud is in the early stages of collapse and still optically thin. Once collapse renders the bulk of the cloud opaque to external photons its effects are negligible and the other three mechanisms are more significant. However in the final stages of collapse direct thermal desorption of grain mantles takes place and this outstrips all four continuous desorption mechanisms. The rate of evaporation is given by (Hasegawa et al. 1992) :

$$k_{\text{evap}} = \nu_0 \exp \left(\frac{-E_D}{kT} \right) \quad (9)$$

For those species that are not mobile on the surface default values are $\nu_0 = 10^{12} \text{s}^{-1}$ and $E_b = 2,000 \text{K}$.

2.4. Reaction set

The basic gas phase reactions are chosen to give a representative model of an interstellar cloud. Beginning with the UMIST astrochemical reaction rates database, RATE95 (Millar et al. 1997), all reactions involving chlorine, phosphorus, iron, silicon, sodium and sulphur are removed along with those involving species with five or more carbon atoms. This yields a reaction set based on hydrogen, helium, carbon, oxygen and nitrogen. Magnesium reactions are included to ensure a “token metal” and source of electrons. Additional provision is made for species formed only on grain surfaces which can pass into the gas phase. An extra set of reactions allowing gas phase destruction of these species has been added to the gas phase reaction set, listed in the Appendix (Table 18).

The surface phase reaction set (Table 18) is constructed with reference to those reactions provided by Hasegawa et al. (1992) and Hasegawa & Herbst (1993). However it is very much optimized to allow the production of $\text{*CH}_3\text{OH}$, $\text{*C}_2\text{H}_5\text{OH}$ and

$\text{*CH}_3\text{OCH}_3$. The reactions listed by Hasegawa et al. contain a number of laboratory measured potential energy barriers which slow down the rate of formation of particular species. Only a few such barriers are used here. Further, the reaction set includes almost entirely reactions orientated to the formation of complex molecules. More reactions to produce other species would reduce the complex molecule abundance by draining “raw material”. It is recognized that this orientation of the reaction set is a limitation of the Gas/Surface model. However, it is regarded as a valid test of the hypothesis of complex molecule formation on grain surfaces. If, given all these advantages, such molecules still could not be produced by grain surface catalysis then the original supposition of such a production method would have to come under deeper scrutiny.

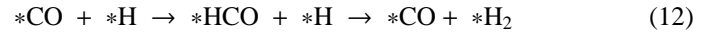
A small number of surface reactions are included that are not directly involved in complex molecule formation. These are included because they are believed to be significant to overall surface chemistry. The most basic of all is the grain formation of H_2 , whose equation is :



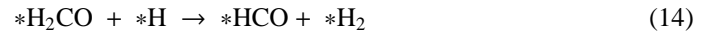
It is considered that the H_2 molecule produced passes directly into the gas phase without the need for any specific desorption process. This is consistent with quantum calculations which indicate the resultant molecule is formed with sufficient energy to eject it directly from the surface. Other reactions form small molecules which are frequently seen in high abundances in regions where grain mantles are thought to have recently evaporated. The basis of nitrogen chemistry is formation of *NH_3 by the route :



Direct combination of atoms can also form *CN , *NO , *HNO , *HCN and *HNC . *O_2 and *OH can also form directly and *OH can further react to form $\text{*H}_2\text{O}$. Other combination reactions allow the formation of *CO and *CH_4 . *CO and *H can also react to form *HCO and *H_2 :



$\text{*H}_2\text{CO}$ can be formed and destroyed by the reactions :



There are two possible routes to *CO_2 , which is stable on the grain surface and does not react further :

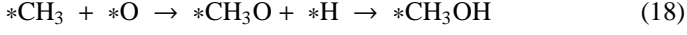


Direct combination of *CO with *O has been omitted as it is believed that this reaction is extremely inefficient (Grim & d’Hendecourt 1986; Breukers 1991). Direct combination of carbon atoms to form *C_2 has also been omitted to simplify the surface chemistry. If it occurred it would lead by hydrogenation to the presence of significant amounts of $\text{*C}_2\text{H}_6$, not currently detected. C_2H_6 is seen in the cometary coma of comets Hyakutake and Hale-Bopp (Mumma et al. 1996) and it is not known if this formed on the surface or in the gas phase. The bulk of surface reactions comprise routes to the complex molecules $\text{*CH}_3\text{OH}$,

*C₂H₅OH and *CH₃OCH₃. *CH₃OH is formed by combining *CH_n and *OH (n = 0-3) :



The resultant is then hydrogenated as necessary to form *CH₃OH. Alternative routes are provided by :



*COH can then hydrogenate. Reaction between *CO and *H can also produce *HCO and the ratio of the two reactions is controlled by activation energy barriers. Routes to *C₂H₅OH and *CH₃OCH₃ involve forming a “spine” of C-C-O or C-O-C and then hydrogenating until the molecule saturates. This is accomplished by the reactions :



Activation energy barriers can be included which slow down particular reactions. Some are from laboratory measurements. (See Hasegawa et al. (1992) and references therein.) Those for the production of *CO₂ (eqns. 15 & 16 above), *CCO (eqn. 20 above) and *COC (eqn. 21 above) have been set to prevent major overabundances of these species. A full list of all surface reactions, with applicable activation energies, is given in the Appendix (Table 18). It is recognized that the surface reaction set used is an approximation. It is constructed by interpolating between measured surface reactions, known or suspected processes in surface chemistry and the aimed-for result of producing complex molecule abundances and a grain mantle composition compatible with observations.

2.5. Species set and starting abundances

The species set is derived from the reaction set. (Full listing in the Appendix, Tables 16 and 17.) All species can exist in the gas phase while only neutral species exist on the grain surface. Any ion freezing out is assumed to be neutralized. For ions with no neutral equivalent it is assumed they break up in exactly the same way as by electron neutralization in the gas phase. The starting abundances (Table 3) are from Hasegawa et al. (1992). Originally used by Leung et al. (1984) they are believed to be a reasonably accurate representation of the abundances found in an interstellar cloud, particularly one liable to collapse into a hot core or hot corino. Earlier gas phase only models derived using them are consistent with observations within the known accuracy of the chemistry.

Table 3. Gas/Surface model - starting abundances

Species	Abundance w.r.t. (H + H ₂)
H	1.00
He	1.40×10^{-1}
C	7.30×10^{-5}
O	1.76×10^{-4}
N	2.14×10^{-5}
Mg	7.00×10^{-9}

3. Model Parameters

3.1. Calculating parameters

As used here only four physical parameters are varied to model cloud collapse : density, visual extinction, gas temperature and grain temperature. All other parameters can be regarded as fixed and their values are given in Table 4. The definitive factor is density, which controls the speed of collapse. In all cases here the cloud is assumed to be spherical and of uniform density. This is recognized as an approximation, possible effects of non-uniform density in star forming clouds are discussed by Shu et al. (1993). For the cloud to begin to contract under its own self-gravity its mass must exceed the Jeans mass (M_J) for its density. For the cloud densities modelled, the masses and corresponding Jeans mass are shown in Table 5, which also gives the relevant free-fall times (t_{ff}) and radii.

The cloud collapse is halted at a density of 10^8 cm^{-3} , observations of hot cores and hot corinos yield densities 10^6 - 10^9 cm^{-3} . As the data in the Appendix demonstrate, by the end of the collapse all the hydrogen in the cloud has become molecular. (H_2 abundance = 5.0×10^{-1} with respect to total hydrogen.) A_V is calculated from Brown (1988) and its increase is stopped at 60 magnitudes as further increases in have negligible effect on the chemistry.

All cloud collapse models presented here assume that gas and grain temperature are the same. Since the gas and grains are closely coupled and the temperature mainly varies as a smooth function it is unlikely that they would be significantly different over the temperature region where the grains have mantles. As a cloud collapses gravitational energy liberated can be efficiently radiated in the infrared and submillimeter bands (Dyson & Williams 1980). However, at some point the temperature must rise to begin nuclear processing. It is assumed that below a density of 10^6 cm^{-3} the cloud can efficiently radiate and temperature (T) in this region is found from a curve fitting technique derived by Tarafdar et al. (1985) :

$$T = \frac{163}{2.5 + \log_e(n) - \log_e(1 + 500\exp(-1.8A_V))} \quad (22)$$

where n is number density and A_V visual extinction. Above $n = 10^6 \text{ cm}^{-3}$ the temperature is determined by the release of gravitational energy :

$$T = T_o \left(\frac{n}{n_o} \right)^{\frac{1}{5}} \quad (23)$$

where T_o is the temperature at 10^6 cm^{-3} . From Tarafdar et al. $T_o = 10 \text{ K}$ and $n_o = 10^6 \text{ cm}^{-3}$. The final temperature obtained is $T = 46.4 \text{ K}$ at the maximum number density $n = 10^8 \text{ cm}^{-3}$. The final environments produced by the models have a temperature of $T = 46.4 \text{ K}$, a number density $n = 10^8 \text{ cm}^{-3}$, an A_V of 60 mags and all remaining hydrogen molecular.

Recently a number of “hot corinos” (Ceccarelli et al. 2004, Bottinelli et al. 2004) have been investigated. These are regions of low mass ($\approx 1 M_\odot$) star formation embedded within and condensed from molecular clouds. They have typical sizes of $\leq 200 \text{ AU}$, temperatures of $\approx 100 \text{ K}$ and densities of $\geq 10^7 \text{ cm}^{-3}$. (Cazaux et al. 2003, Bottinelli et al. 2004 and references within.) Complex molecules have been detected in four hot corino sources, listed in Table 1.

Table 4. Gas/Surface model - fixed parameters

Parameter	Value	Ref.
UV Radiation field	$3.0 \times 10^8 \text{ cm}^{-2} \text{ s}^{-1} \text{ Hz}^{-1}$	1
Cosmic ray ionization rate	$1.3 \times 10^{-17} \text{ s}^{-1}$	2
Grain albedo	0.5	3
Sticking coefficient	1.0	4
Sticking coefficient for hydrogen atoms	0.3	5
Yield per UV photon on grain mantle impact	10^{-6}	6
Surface density of sites	$1.5 \times 10^{15} \text{ cm}^{-2}$	4
Number of sites per grain	10^6	4
Fractional density of grains (w.r.t. Density of H)	1.33×10^{-12}	4
Average grain radius	10^{-5} cm	4
Barrier width between adjacent sites	10^{-8} cm	4
Grain velocity (non-thermal)	10^4 cm s^{-1}	7

References. (1) Draine 1978; (2) van Dishoeck & Black 1986; (3) Whittet 1992; (4) Hasegawa et al. 1992; (5) Brown 1988; (6) Willacy 1993; (7) Völk et al. 1980;

Table 5. Gas/Surface model - cloud parameters

Initial Number Density (cm^{-3})	Mass (M_\odot)	M_J (M_\odot)	t_{ff} (years)	Initial Radius (parsecs)	Final Radius (parsecs)	Initial A_v (Mag)	Initial Temp. (K)
100	1700	1692.7	4.40×10^6	5.0818	0.065	1.39	48.5
1,000	150	144.3	1.39×10^6	1.0501	0.034	2.86	20.2
10,000	26	25.97	4.40×10^5	0.2717	0.006	7.41	13.9

Table 6. Collapse scenario model parameters

	Initial Number Density (cm^{-3})	Parameter	Minimum Temperature	Plateau Point
Model 1	100	Time (yrs)	4.36×10^6	4.39×10^6
Free-fall	Atomic	n (cm^{-3})	6.97×10^5	1.00×10^8
Model 2	1,000	Time (yrs)	1.36×10^6	1.39×10^6
Free-fall	Atomic	n (cm^{-3})	6.78×10^5	1.00×10^8
Model 3	10,000	Time (yrs)	4.18×10^5	4.38×10^5
Free-fall	Atomic	n (cm^{-3})	9.47×10^5	1.00×10^8
Model 4	100	Time (yrs)	2.18×10^7	2.19×10^7
Retarded ($\times 5$)	Atomic	n (cm^{-3})	1.00×10^6	1.00×10^8
Model 5	1,000	Time (yrs)	6.84×10^6	6.93×10^6
Retarded ($\times 5$)	Atomic	n (cm^{-3})	9.87×10^5	1.00×10^8
Model 6	10,000	Time (yrs)	2.07×10^6	2.19×10^6
Retarded ($\times 5$)	Atomic	$n(\text{cm}^{-3})$	7.73×10^5	1.00×10^8
Model 7	10,000	Time (yrs)	4.18×10^5	4.38×10^5
Free-fall	Molecular	n (cm^{-3})	9.47×10^5	1.00×10^8
Model 8	10,000	Time (yrs)	2.07×10^6	2.19×10^6
Retarded ($\times 5$)	Molecular	$n(\text{cm}^{-3})$	7.73×10^5	1.00×10^8

3.2. Collapse scenarios

In all, eight different cloud collapse scenarios are investigated, designated models 1-8. Models 1-3 are free-fall collapses with starting abundances of 100, 1,000 and $10,000 \text{ cm}^{-3}$, regarded as slow, medium and fast. The observed formation rate of new stars is too low for all stars in the galaxy to be formed by free-fall collapse. It is widely asserted that some mechanism supports clouds against collapse, the most commonly suggested being magnetic fields (Shu et al. 1993). For this reason models 4-6 are retarded collapses, again with starting abundances of 100, 1,000 and $10,000 \text{ cm}^{-3}$. No specific retardation mechanism is incorporated in the Gas/Surface model nor is one necessary. Retardation is accounted for by arbitrarily slowing down the decrease in radius by a factor of 5.0. This ensures that the cloud takes longer to collapse with corresponding further evolution in the chemistry. Apart from retardation the parameter change in density, gas and

grain temperature and visual extinction follows exactly the same pattern as in models 1-3.

For the purposes of direct comparison as many parameters as possible are kept constant for all collapses. At a density of 100 cm^{-3} the hydrogen is likely to be almost completely atomic. Observed clouds of this density are optically thin and exposure to background starlight ensures an ample supply of UV photons to break up H_2 . At $1,000 \text{ cm}^{-3}$ this is still approximately true though some H_2 does form. However at the high density case of $10,000 \text{ cm}^{-3}$ it is unphysical. The clouds are sufficiently dense that they will be predominantly H_2 . For this reason the final models, 7 and 8, replicate the free-fall and retarded collapses from $10,000 \text{ cm}^{-3}$ with their initial hydrogen abundance molecular instead of atomic.

Essentially the chemistry during cloud collapse can be divided into three approximate segments :

1. Pre-freeze out. Gas phase chemistry dominates, similar to that in gas phase only models.
2. Freeze out. As the temperature falls and the visual extinction (A_V) increases (curtailing photodesorption), freeze out occurs and surface reactions dominate the chemistry. This occurs around the minimum temperature, ≈ 10.0 and 10.2 K.
3. Post-freeze out. Once the temperature rises the entire grain mantle passes back into the gas phase. Grain surface products are suddenly released into a very dense, warm, dark cloud environment. This leads to a rapidly changing chemistry where a wide variety of different species interact.

Table 6 lists the parameter values for each model at the beginning of its run, the point of minimum temperature and the “plateau point”. The plateau point is where parameter change ceases. In all cases at the plateau point the density is 10^8 cm^{-3} , temperature 46.4 K and visual extinction 60.0 magnitudes. For the 2.0×10^5 years beginning at the plateau point each model most closely represents the chemistry of a hot corino. All model runs terminate 2.0×10^5 years after the plateau point is reached.

4. Discussion

The Appendix contains output data from each of the eight models. The most abundant gas phase species at both the plateau point and 2.0×10^5 years later are listed in Tables 19 - 26. Variation in gas phase species abundance over time is shown in Figures ?? - 8. The results are discussed in this section.

4.1. Mantle composition

The test of any theoretical model is to compare it to observations. Table 7 presents observational data on interstellar ices towards a number of sources. The abundances shown are relative to H_2O and have been measured by Boogert et al. (2008) for HCOOH & CH_3OH , Pontoppidan et al. (2008) for CO & CO_2 , Öberg et al. (2008) for CH_4 and Gibb et al. (2000) for NH_3 & H_2CO . For data taken from Boogert et al. (2008) measured values have been taken, observations where a lower limit only has been established have been omitted. Further Boogert et al. (2008) data for NH_4^+ has been omitted as the authors themselves point out that the inclusion of certain components in the abundance estimation is still a matter of debate.

It is assumed that ice measurements reflect the composition of grain mantles along the measured lines of sight. No measurements are available for mantles in hot cores or hot corinos as within these regions the temperature is sufficiently high that any grains have been fully thermally desorbed. Observations made of other, cooler regions are therefore the best available indicator of grain mantle composition. All models produce mantles with a predominance of H_2O , (absolute composition 40-64%), agreeing with observations. Table 8 presents mantle composition at greatest thickness as a percentage of H_2O abundance for all mantle species with abundance $\geq 1\%$ H_2O and for the complex molecules regardless of their contribution. Table 9 shows the conditions during each model when the mantle is at its greatest thickness. The point of greatest thickness is defined as that timestep with the largest number of surface layers. Where this is the same for two or more timesteps the latest is taken.

CO is well modelled in models 1-4 and 6 and overproduced in the other three. For models 7 and 8 this is a consequence of the molecular hydrogen starting abundance. In both cases atomic carbon and oxygen are able to preferentially combine with each

other due to the absence of atomic hydrogen which would otherwise convert them to H_2O and CH_4 . Model 5 appears to be an optimum case (with initial atomic hydrogen) for the production of CO and also subsequently $\text{C}_2\text{H}_5\text{OH}$ and CH_3OCH_3 , hence the higher proportion of all three of these species. Table 10 bears this out, showing an order of magnitude lower carbon abundance at freeze out time in model 5 compared to the other models. Correspondingly both CO and CO_2 are significantly more abundant in model 5. Both these are preferentially formed in the gas phase before freeze out. CO_2 is well modelled in models 4, 5, 7 and 8 and underproduced in all others. Again in models 7 and 8 the absence of initial atomic hydrogen is the major factor here, while in models 4 and 5 it seems that the longer time period before freeze out enhances CO_2 production, for the same reasons as it also enhances CO production. Exactly the same factors result in CH_4 being well modelled in models 5, 7 and 8 and overproduced in all others. The faster collapses (models 1, 2, 3 and 6) freeze out atomic carbon before it can form molecules in the gas phase and once on the grain this rapidly hydrogenates into CH_4 . Model 4 then appears as a transitory case. It has more CH_4 than model 5, about the same as the faster cases, with correspondingly more CO and CO_2 than the faster cases and less than model 5. It appears that for model 4 the greater time before freeze out for CO and CO_2 to form is partially offset by the lower starting density. The same effect can be seen when comparing models 1 and 2, though it is not as pronounced.

NH_3 is well modelled in models 1, 2 and 3, above the 1% threshold in model 7 and underproduced in the other models. Here it seems that rapid collapse alone is the major factor. Abundance in model 7 is significantly lower than in models 1-3, entirely a consequence of the molecular hydrogen starting abundance. Models 4-8 all predict $\geq 1\%$ HNO . Correspondingly these are the models with the least NH_3 . The highest HNO abundance is in models 7 and 8, again a consequence of the molecular hydrogen starting abundance. Nitrogen cannot easily form NH_3 in the gas or surface phase due to the lack of atomic hydrogen. Instead, atomic nitrogen freezes out and combines with OH to form HNO . The lack of atomic hydrogen allows there to be proportionately more OH available, which otherwise would hydrogenate to form H_2O . Models 4 and 5 seem to be intermediate cases, their longer collapse times allowing some but not all of the initial gas phase atomic hydrogen to convert to molecular before freeze out.

HNO is not currently observed in grain mantles and is another model prediction to be searched for. However its greatest abundance occurs in two collapses (models 7 and 8), both with high starting density. A dense cloud with ample molecular hydrogen could have evolved chemically before collapse begins reducing the HNO abundance by enabling atomic nitrogen to combine into other species in the early gas phase. All models predict a significant mantle abundance of N_2 and most models O_2 , at $\approx 10\%$. In the absence of observational measurements these must be regarded as model predictions. Ehrenfreund & van Dishoeck (1998) suggest possible ways of searching for N_2 and O_2 while Ehrenfreund & Schutte (2000) describe the current state of observations.

Although mantle composition observations cannot be regarded as complete and definitive, approximate agreement for H_2O and CO is seen in mantles produced by the Gas/Surface model. Mantle compositions in models 3 and 6 ($10,000 \text{ cm}^{-3}$ free fall and retarded) must be regarded as suspect as it is likely that the scenarios themselves are unphysical, starting as they do from atomic hydrogen. Models 4, 5, 7 and 8 produce composi-

Table 7. Observed interstellar ices (See text for references)

Source	*H ₂ O	*HCOOH	*CH ₃ OH	*CH ₄	*CO ₂	*CO	*NH ₃	*H ₂ CO
B1-b	100.00	3.1	11.2	3.3				
IRAS 08242-5050	100.00	2.7	5.5	5.0				
IRAS 15398-3359	100.00	1.9	10.3	6.0	35.24	5.63		
SVS 4-5	100.00	4.6	25.2	6.1	30.46	13.09		
L1014 IRS	100.00	5.4	3.1	7.1				
W33A	100.00	5.2	14.7		12.49	7.37	15.0	6.0
GL 2136	100.00	5.1	8.5		13.24	10.19		
GL 7009S	100.00	2.5	31.3					
NGC7538 IRS9	100.00		7.5				13.0	4.0

Table 8. Mantle composition w.r.t H₂O at maximum mantle thickness for each model

Species	Model 1	Model 2	Model 3	Model 4	Model 5	Model 6	Model 7	Model 8
*H ₂ O	100.00	100.00	100.00	100.00	100.00	100.00	100.00	100.00
*CH ₄	34.23	28.62	32.50	28.34		31.51	3.08	2.45
*NH ₃	5.94	3.88	5.04				1.14	
*N ₂	3.75	5.60	4.39	7.87	13.76	6.31	8.46	10.50
*CO	3.65	7.15	3.88	14.73	69.53	4.42	55.66	71.91
*CO ₂		1.69		7.16	24.46	2.22	22.12	28.43
*O ₂	1.24			5.65	12.79	2.17	2.77	15.49
*HNO				1.92	3.71	1.45	9.16	11.68
*C ₄ H								1.17
*CH ₃ OH	7.98	14.70	11.46	10.32	12.12	13.05	1.91	1.57
*C ₂ H ₅ OH	1.19×10^{-3}	7.74×10^{-4}	7.64×10^{-4}	9.50×10^{-4}	1.28×10^{-3}	6.21×10^{-4}	3.49×10^{-2}	2.43×10^{-2}
*CH ₃ OCH ₃	5.80×10^{-7}	2.60×10^{-7}	2.10×10^{-7}	9.00×10^{-8}	9.47×10^{-5}	5.50×10^{-7}	2.24×10^{-4}	1.05×10^{-4}

Table 9. Mantle layering

		Model 1	Model 2	Model 3	Model 4
Maximum	Layers	184	169	179	154
Thickness	Time (years)	4.38×10^6	1.38×10^6	4.28×10^5	2.19×10^7
	Density (cm ⁻³)	5.95×10^6	5.02×10^6	3.39×10^6	5.62×10^6
	Temperature (K)	18.1	17.1	15.0	17.8
		Model 5	Model 6	Model 7	Model 8
Maximum	Layers	121	169	126	119
Thickness	Time (years)	6.90×10^6	2.14×10^6	4.28×10^5	2.14×10^6
	Density (cm ⁻³)	8.81×10^6	3.20×10^6	3.39×10^6	3.20×10^6
	Temperature (K)	20.7	14.7	15.0	14.7

tions closest to observations, although models 7 and 8 predict *CH₃OH abundance at the low end of its observed abundance range. The effects of collapse timescale on mantle composition are shown in Table 10 which lists relative abundances of gas phase C, CO, CO₂, H, H₂ and O with respect to total hydrogen at the beginning of freeze out. This is arbitrarily defined, for the purposes of this discussion, as the last timestep before at least five mantle layers form on the grain. Models 2, 4 and particularly 5 seem to have an optimum combination of collapse speed and density to allow significant CO to form in the gas phase. This partially depletes atomic carbon and enables freeze out to occur while there is still some atomic hydrogen available with corresponding consequences for the chemistry thereafter.

4.2. Complex molecules

4.2.1. Complex molecules - surface phase

The prime function of the Gas/Surface model is to investigate the formation of complex molecules by grain surface catalysis. Gas phase abundances in the final stages of collapse are governed by surface abundances prior to mantle desorption. The mantle abundances with respect to *H₂O of *CH₃OH, *C₂H₅OH and

*CH₃OCH₃ at the greatest mantle thickness for each model are listed in Table 8. Models 1-6 all produce *CH₃OH in the 5-15% range, agreeing well with observations. Models 7 and 8 produce $\approx 1\%$. This is a consequence of the initial hydrogen being molecular. *CH₃OH requires atomic hydrogen for its formation (Section 2.4) and with little available formation is significantly reduced.

Models 1-6 all produce about the same amount of *C₂H₅OH ($\approx 0.001\%$) while models 7 and 8 produce significantly more ($\approx 0.025\%$). For *CH₃OCH₃ models 1-4 and 6 produce $\approx 0.0000002\%$ while models 5, 7 and 8 production is higher at $\approx 0.0001\%$. Formation of complex molecules requires atomic carbon and *CO on the grain, the *CO originating in the gas phase (Section 2.4). Maximum production takes place when the prior gas phase has produced significant CO, while leaving sufficient atomic carbon to form C-C-O and C-O-C structures on the surface after freeze out. At the same time if there is considerable atomic hydrogen present at freeze out then this will rapidly hydrogenate atomic carbon on the grain surface leaving little available to form complex molecules. This is demonstrated by models 7 and 8 where the initial hydrogen is entirely molecular. Absence of much atomic hydrogen leaves CO to form preferentially in the gas phase. It then freezes out alongside atomic car-

Table 10. Gas phase abundances - freeze out

	Time (years)	C	CO	CO ₂	H	H ₂	O
Model 1	3.67×10^6	6.76×10^{-5}	8.34×10^{-7}	7.95×10^{-14}	7.79×10^{-1}	1.11×10^{-1}	1.71×10^{-4}
Model 2	7.94×10^5	5.81×10^{-5}	1.27×10^{-5}	3.97×10^{-11}	7.64×10^{-1}	1.18×10^{-1}	1.61×10^{-4}
Model 3	1.25×10^4	6.99×10^{-5}	9.23×10^{-7}	1.07×10^{-12}	9.73×10^{-1}	1.33×10^{-2}	1.71×10^{-4}
Model 4	1.81×10^7	5.67×10^{-5}	1.13×10^{-5}	1.46×10^{-11}	3.10×10^{-1}	3.45×10^{-1}	1.60×10^{-4}
Model 5	4.42×10^6	3.69×10^{-6}	6.55×10^{-5}	3.69×10^{-7}	2.20×10^{-1}	3.90×10^{-1}	9.64×10^{-5}
Model 6	1.25×10^4	6.99×10^{-5}	9.23×10^{-7}	1.07×10^{-12}	9.73×10^{-1}	1.33×10^{-2}	1.71×10^{-4}
Model 7	2.51×10^4	6.08×10^{-5}	6.07×10^{-6}	5.95×10^{-9}	3.48×10^{-5}	5.00×10^{-1}	1.61×10^{-4}
Model 8	2.51×10^4	6.08×10^{-5}	6.06×10^{-6}	5.94×10^{-9}	3.47×10^{-5}	5.00×10^{-1}	1.61×10^{-4}

Table 11. Complex molecule abundances - gas phase

	Abundance w.r.t. H + H ₂					
	CH ₃ OH	C ₂ H ₅ OH		CH ₃ OCH ₃		
	Plateau Point	Plateau Point + 2.0×10^5 yrs	Plateau Point	Plateau Point + 2.0×10^5 yrs	Plateau Point	Plateau Point + 2.0×10^5 yrs
Model 1	1.12×10^{-5}	4.32×10^{-7}	1.78×10^{-9}	1.45×10^{-8}	3.01×10^{-7}	8.36×10^{-7}
Model 2	1.83×10^{-5}	3.80×10^{-7}	1.04×10^{-9}	3.32×10^{-8}	4.11×10^{-7}	5.81×10^{-7}
Model 3	1.55×10^{-5}	5.23×10^{-7}	1.11×10^{-9}	1.26×10^{-8}	3.63×10^{-7}	1.04×10^{-6}
Model 4	8.56×10^{-6}	7.98×10^{-8}	1.69×10^{-9}	6.21×10^{-8}	8.61×10^{-7}	6.86×10^{-8}
Model 5	5.44×10^{-6}	1.34×10^{-9}	1.40×10^{-9}	6.48×10^{-10}	7.69×10^{-7}	1.62×10^{-11}
Model 6	1.09×10^{-5}	1.66×10^{-7}	1.76×10^{-9}	5.63×10^{-9}	1.64×10^{-6}	1.92×10^{-7}
Model 7	8.71×10^{-7}	2.72×10^{-9}	2.30×10^{-8}	4.76×10^{-10}	1.94×10^{-7}	7.07×10^{-11}
Model 8	1.51×10^{-7}	1.97×10^{-9}	9.32×10^{-9}	2.73×10^{-10}	1.27×10^{-7}	3.94×10^{-11}

Table 12. Molecular abundance in a sample of four low-mass protostars (Bottinelli et al. 2007)

Molecule	IRAS16293-2422	NGC1333-IRAS4A	NGC1333-IRAS4B	NGC1333-IRAS2A	Ref.
H ₂ CO	1.0×10^{-7}	2.0×10^{-8}	3.0×10^{-6}	2.0×10^{-7}	1,2,3
CH ₃ OH	1.0×10^{-7}	$< 1.0 \times 10^{-8}$	7.0×10^{-7}	3.0×10^{-7}	4
HCOOCH ₃ -A	1.7×10^{-7}	3.4×10^{-8}	1.1×10^{-6}	$< 6.7 \times 10^{-7}$	5,2,6
HCOOH	6.2×10^{-8}	4.6×10^{-9}	$< 1.0 \times 10^{-6}$	$< 1.2 \times 10^{-7}$	5,2,6
CH ₃ OCH ₃	2.4×10^{-7}	$< 2.8 \times 10^{-8}$	$< 1.2 \times 10^{-6}$	3.0×10^{-8}	5,2,6,7
CH ₃ CN	1.0×10^{-8}	1.6×10^{-9}	9.5×10^{-8}	8.7×10^{-9}	5,2,6
C ₂ H ₅ CN	1.2×10^{-8}	$< 1.2 \times 10^{-9}$	$< 7.5 \times 10^{-7}$	$< 1.0 \times 10^{-7}$	5,2,6

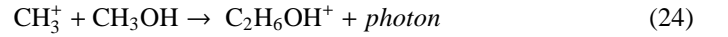
References. (1) Ceccarelli et al. 2000; (2) Bottinelli et al. 2004; (3) Maret et al. 2004; (4) Maret et al. 2005; (5) Cazaux et al. 2003; (6) Bottinelli et al. 2007; (7) Jørgensen et al. 2005

bon which cannot readily hydrogenate into CH_4 and so is available to form C-C-O and C-O-C. Models 7 and 8 show low CH_4 , enhanced CO and the largest proportions of both $\text{C}_2\text{H}_5\text{OH}$ and CH_3OCH_3 .

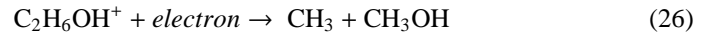
Models 1, 2, 3 and 6 with their faster collapse times and initial atomic hydrogen all have significantly lower CO in the mantle and hence much lower complex molecule abundance. Models 4 and 5 have the longest collapse time of any of the models. This leads to significantly more CO , in the case of model 5 approximately the same as in the molecular hydrogen starting abundance cases. Model 4 again appears as a transitory case. It has 15% CO , formed in the gas phase and then frozen out. However its initial low density means that significant atomic hydrogen is present at freeze out and this can hydrogenate the remaining atomic carbon to CH_4 (28%) leaving very little for the production of complex molecules. Model 5 avoids this situation. Here substantial CO is frozen out but very little atomic hydrogen remains, hence the paucity of CH_4 . Much of the remaining carbon has contributed to the high CO_2 abundance (also seen in models 7 and 8) however some has led to the significantly increased CH_3OCH_3 .

Each model produces a higher mantle abundance for $\text{C}_2\text{H}_5\text{OH}$ than CH_3OCH_3 . For models 1-4 and 6 the difference is greater than 3 orders of magnitude while for models 7

and 8 it is 2 and for model 5 only 1. The abundance difference seems to be caused by reaction channel differences. $\text{C}_2\text{H}_5\text{OH}$ forms mainly by hydrogenation on the grain of C-C-O. However CH_3OCH_3 seems to form mainly by freeze out from the gas phase. Its gas phase origin is a two stage process with $\text{C}_2\text{H}_6\text{OH}^+$ (protonated dimethyl ether) as an intermediate :



Gas phase $\text{C}_2\text{H}_6\text{OH}^+$ can also be destroyed by :



Essentially $\text{C}_2\text{H}_6\text{OH}^+$ is made from CH_3OH . Once formed it is then destroyed in forming CH_3OCH_3 (eqn. 25) which can freeze out onto the grain surface where it is stable or it can form CH_3OH (eqn. 26) which is then available to form more $\text{C}_2\text{H}_6\text{OH}^+$ via eqn. 24. As long as the temperature is low enough to ensure that there is a net freeze out of molecules onto the grain surface this process results in a build up of CH_3OCH_3 . While workable this gas phase production of CH_3OCH_3 which then freezes out is less efficient than the direct grain surface hydrogenation which produces $\text{C}_2\text{H}_5\text{OH}$ in significantly greater

abundances. Although production of $\text{C}_2\text{H}_5\text{OH}^+$ takes place in the gas phase grain surface catalysis is crucial to the process. At the time of freeze out most CH_3OH is being produced by evaporation from the grain mantle. In turn the dominant production of $\text{*CH}_3\text{OH}$ is by a chain of direct hydrogenation reactions of *CO .

Comparison of reaction rates of complex molecule formation for the different models shows that model 5 seems to have an optimum combination of parameters to form $\text{*CH}_3\text{OCH}_3$, hence its significantly higher abundance in this model. Table 1 does not show any consistency in $\text{C}_2\text{H}_5\text{OH} : \text{CH}_3\text{OCH}_3$ ratio and it seems from the models here that the abundance ratio of these two is significantly sensitive to prevailing conditions.

4.2.2. Complex molecules - gas phase

Table 13. Acceptable gas phase fractional abundance ranges for complex molecules

Molecule	Minimum Abundance	Maximum Abundance
CH_3OH	5.0×10^{-8}	2.0×10^{-6}
CH_3OCH_3	8.0×10^{-9}	7.4×10^{-7}

Other than $\text{*CH}_3\text{OH}$ no observations are currently available of complex molecules in grain mantles. However measurements do exist of gas phase abundances (Table 12) and these can be compared to the results of the models shown in Table 11. Comparisons are made at the plateau point and at 2.0×10^5 years later, the end point of time segment 2. Between these two points the model most closely resembles a hot corino. There are uncertainties in observations and even when these can be minimized apparently similar sources yield significantly different abundance values for the same species. There are further uncertainties in the chemistry both in the processes of surface chemistry and the accuracy of gas phase rate coefficients. For these reasons a model-predicted gas phase abundance is considered to be in reasonable agreement with observations if it falls within half an order of magnitude of the range of observed values at any time between the plateau point and 2.0×10^5 years later. The acceptable ranges for complex molecules are given in Table 13, (derived from Table 12).

CH_3OH is well modelled in all scenarios, though the abundance varies significantly. In all of models 1-6 (all models starting with atomic hydrogen) CH_3OH is overproduced at the plateau point and then for five of these cases falls to within the acceptable range by 2.0×10^5 years later. The sole exception here is model 5 (retarded collapses from $1,000 \text{ cm}^{-3}$) where the abundance actually drops to below the valid range 2.0×10^5 years later. Since the abundance has passed through the valid range during the time period in question this is held to indicate validity. Models 7 & 8 (with molecular hydrogen starting abundance) are both within the valid range at the plateau point and fall below it by 2.0×10^5 years later. In all cases the CH_3OH gas phase abundance declines after the grain mantles are evaporated.

CH_3OCH_3 can also be considered well modelled in all cases, though its behaviour is more diverse. Models 1, 2 & 3 are within acceptable range at the plateau point and by 2.0×10^5 years later abundance has actually increased, suggesting further production in the gas phase. At this time model 2 is still within the acceptable range while 1 & 3 overproduce. Models 4, 5, & 6 all overproduce slightly at the plateau point while 2.0×10^5 years later abundances have dropped to within acceptable range for models

4 & 6 and below acceptable range for model 5. As with CH_3OH model 5 CH_3OCH_3 abundance is considered to be validly modelled as it has passed through the acceptable range during the relevant time period. In this case the precipitous drop, 4 orders of magnitude, serves to illustrate how volatile the chemistry becomes in the period after the grain mantles evaporate. Models 7 & 8 show a similar behaviour being within acceptable range at the plateau point and also dropping by 4 orders of magnitude 2.0×10^5 years later.

As discussed in Sections 4.1 and 4.2.1 the production of complex molecules is dependent on the gas phase abundances of atomic carbon and hydrogen at the point of freeze out. Gas phase processes are considerably better understood than surface processes, and in particular the potential barriers used could be different leading to changes in the relative proportions of species. With these caveats we conclude that complex molecules, seen in both hot cores and hot corinos, can be made in the observed abundances by grain surface catalysis processes. Ethanol ($\text{C}_2\text{H}_5\text{OH}$) production has been included in the models here as it is frequently seen in the same environments as dimethyl ether (CH_3OCH_3) (Table 1). Currently it has not been observed in hot corinos and the abundances modelled here must be regarded as predictions awaiting the test of observation. The only major distinction that can be drawn between the different models is between those starting with molecular hydrogen (models 7 & 8) compared to the other six. As would be expected the lack of initial atomic hydrogen stifles the production of those molecular species which require it. Correspondingly this then allows higher abundances of other species whose “raw material” would otherwise have been removed by combination with atomic hydrogen. No correlation is noticeable in the production of complex molecules in either gas or surface phase with the cloud starting mass and/or collapse time. This may be indicative of a volatile chemistry and/or of the limitations of our current understanding.

Table 12 lists observational measurements for a number of other molecules observed in hot corinos. These too can be compared to the models here as a validity check. HCOOH and $\text{C}_2\text{H}_5\text{CN}$ are not in the Gas/Surface model reaction set as used here.

Both of these two species are obvious candidates for inclusion in future modelling. HCOOH may be particularly significant as both gas (Table 12) and solid phase (Table 7) data are now available for it. Both Bottinelli et al. (2007) and Fuente et al. (2005) point out that HCOOH shows significantly different abundance behaviour between corino type objects, as modelled here, and higher temperature hot cores, unlike a majority of other observed species. The reasons for this are not known but present an interesting issue for prospective future models. H_2CO , HCOOCH_3 and CH_3CN are included and their abundances are listed in Table 15. The same criteria for acceptable range is used as above, namely a gas phase abundance is considered to be in reasonable agreement with observations if it falls within half an order of magnitude of the range of observed values at any time between the plateau point and 2.0×10^5 years later. Relevant values are shown in Table 14.

H_2CO is well modelled in all collapse scenarios. Table 12 lists only abundance data for HCOOCH_3 -A. Bottinelli et al. (2007), from where this data is taken, state that the abundance of the “E” form of HCOOCH_3 is usually very close to that of the “A” form and that they regard the HCOOCH_3 total abundance to be twice that of HCOOCH_3 -A. For this reason the acceptable range of HCOOCH_3 is given in Table 14 as 1.8×10^{-8} - 7.2×10^{-6} , i.e., half an order of magnitude above and below double the HCOOCH_3 -A abundance. Modelled HCOOCH_3 is under-

abundant at the plateau point in all cases. By 2.0×10^5 years later it remains underabundant in seven of the eight cases. Only in model 2 does it rise above the acceptable lower limit. CH_3CN is well modelled in most of the cases. In models 1-4 & 6 it is within the acceptable range both at the plateau point and 2.0×10^5 years later. In models 5 & 8 it is always underabundant. In model 7 it is within acceptable range at the plateau point and has fallen to below it by 2.0×10^5 years later. For all three of these molecules there is no discernible correlation between abundance produced and cloud starting mass and/or collapse time.

5. Conclusion

Overall the Gas/Surface model as used here reproduces to a reasonable degree the observed complex molecule abundances seen in hot corinos. In particular abundance values produced for methanol and dimethyl ether are comparable to those observed in both gas and surface phases.

The surface phase molecular abundances produced by the model reflect the starting conditions, particularly the nature of the initial hydrogen - atomic or molecular. This determines the degree of processing in the initial gas phase and hence the abundance of species frozen on to the dust and available for surface chemistry. This in turn allows an understanding of the differences in grain mantle composition observed in different regions. The model results clearly indicate that both the starting conditions and particularly the timescale of collapse are major contributors to the overall chemistry.

A number of other workers in the area have reached similar conclusions. Garrod & Herbst (2006) specifically investigated methyl formate (HCOOCH_3). They concluded that its formation required the grain surface production of precursor molecules which were then released into the gas phase to produce methyl formate itself. This tallies with the similar behaviour seen here although Garrod & Herbst were able to produce abundances closer to observed values. They suggest a similar pattern for dimethyl ether, exactly as the Gas/Surface model shows. Later applications of the same model produced comparable results. Aikawa et al. (2008) consider a collapse case where again large organic species (or their immediate precursors) are formed on grain mantles before evaporation into the gas phase. Observed abundances can be both well modelled or over and under produced depending on starting conditions and timescale. Garrod et al. (2008) apply their model to more general star formation cases and note specifically that the longer the time available for grain surface chemistry to progress the more complex the eventual gas phase chemistry becomes. In this case agreement with observations is seen for abundances of ethanol and dimethyl ether though not for some other complex molecules. Hassel et al. (2008) specifically model L1529, a “lukewarm” corino, which may be the prototype of a new class of such objects. Their analysis demonstrates that, at least in the case of L1529, there is some difficulty in establishing definitively how a particular chemical state came to evolve and a number of scenarios are possible depending on the length of time the corino spent in each particular phase.

In conclusion then grain surface processing, combined with the variation of physical conditions modelled here, can be regarded as a viable method for the formation of complex molecules, particularly ethanol and dimethyl ether, in the environment found in the vicinity of a hot corino and produce abundances comparable to those actually observed.

Acknowledgements. Astrophysics at Queens University Belfast is supported by a grant from STFC. P. Hall wishes to thank Professor H. Fleischmann of Cornell

University Department of Applied and Engineering Physics for helpful conversations about optical absorption. We both wish to thank an anonymous referee whose comments improved an earlier version of this paper.

Appendix - Model Data

Table 14. Acceptable gas phase abundance ranges for other molecules

Molecule	Minimum Abundance	Maximum Abundance
H ₂ CO	7.0×10^{-9}	8.0×10^{-6}
HCOOCH ₃	1.8×10^{-8}	7.2×10^{-6}
CH ₃ CN	6.6×10^{-10}	4.5×10^{-7}

Table 15. Other molecule abundances - gas phase

	Abundance w.r.t. H + H ₂					
	H ₂ CO		HCOOCH ₃		CH ₃ CN	
	Plateau Point	Plateau Point + 2.0×10^5 yrs	Plateau Point	Plateau Point + 2.0×10^5 yrs	Plateau Point	Plateau Point + 2.0×10^5 yrs
Model 1	2.95×10^{-07}	2.05×10^{-08}	4.83×10^{-11}	1.52×10^{-09}	4.20×10^{-09}	1.92×10^{-07}
Model 2	4.37×10^{-07}	1.77×10^{-06}	6.12×10^{-11}	2.19×10^{-08}	2.44×10^{-09}	2.85×10^{-08}
Model 3	3.88×10^{-07}	2.23×10^{-08}	5.57×10^{-11}	2.68×10^{-09}	2.56×10^{-09}	1.53×10^{-07}
Model 4	8.56×10^{-07}	4.62×10^{-06}	4.90×10^{-10}	1.33×10^{-08}	1.64×10^{-09}	1.61×10^{-09}
Model 5	5.32×10^{-07}	4.52×10^{-07}	3.60×10^{-10}	7.18×10^{-11}	4.05×10^{-10}	5.05×10^{-13}
Model 6	2.00×10^{-06}	1.52×10^{-08}	1.67×10^{-09}	3.01×10^{-09}	5.61×10^{-09}	1.75×10^{-08}
Model 7	5.01×10^{-07}	1.61×10^{-07}	9.06×10^{-10}	5.23×10^{-11}	2.34×10^{-09}	2.12×10^{-13}
Model 8	6.70×10^{-07}	2.61×10^{-08}	2.78×10^{-09}	6.82×10^{-12}	2.58×10^{-10}	1.38×10^{-14}

Table 16. Gas/Surface model - surface phase species set

*C	*C ₂	*C ₂ H	*C ₂ H ₂	*C ₂ H ₃	*C ₂ H ₃ O	*C ₂ H ₄	*C ₂ H ₅	*C ₂ H ₅ O	*C ₂ H ₅ OH
*C ₂ H ₆	*C ₂ H ₆ CO	*C ₂ HO	*C ₃	*C ₃ H	*C ₃ H ₂	*C ₃ H ₃	*C ₃ H ₄	*C ₃ N	*C ₃ O
*C ₄	*C ₄ H	*C ₄ H ₂	*CCN	*CCO	*CH	*CH ₂	*CH ₂ CN	*CH ₂ CO	*CH ₂ NH
*CH ₂ OC	*CH ₂ OH	*CH ₃	*CH ₃ CHO	*CH ₃ CN	*CH ₃ O	*CH ₃ OC	*CH ₃ OCH	*CH ₃ OCH ₂	*CH ₃ OCH ₃
*CH ₃ OH	*CH ₄	*CHOC	*CHOH	*CHOOH	*CN	*CO	*CO ₂	*COC	*COH
*H	*H ₂	*H ₂ C ₃	*H ₂ CN	*H ₂ CO	*H ₂ O	*H ₂ O ₂	*H ₃ C ₃ N	*H ₃ C ₄ N	*HC ₃ N
*HCN	*HCO	*HCOOCH ₃	*He	*HNC	*HNO	*Mg	*N	*N ₂	*N ₂ O
*NH	*NH ₂	*NH ₃	*NO	*NO ₂	*O	*O ₂	*O ₂ H	*OCN	*OH

Table 17. Gas/Surface model - gas phase species set

C	C ⁺	C ⁻	C ₂	C ₂ ⁺	C ₂ H	C ₂ H ⁺	C ₂ H ₂	C ₂ H ₂ ⁺	C ₂ H ₃
C ₂ H ₃ ⁺	C ₂ H ₃ O	C ₂ H ₃ O ⁺	C ₂ H ₄	C ₂ H ₄ ⁺	C ₂ H ₄ O ⁺	C ₂ H ₅	C ₂ H ₅ ⁺	C ₂ H ₅ O	C ₂ H ₅ O ⁺
C ₂ H ₅ OH	C ₂ H ₅ OH ⁺	C ₂ H ₆	C ₂ H ₆ ⁺	C ₂ H ₆ CO	C ₂ H ₆ CO ⁺	C ₂ H ₆ O ⁺	C ₂ H ₆ OH ⁺	C ₂ H ₇ ⁺	C ₂ H ₇ O ⁺
C ₂ HO	C ₂ HO ⁺	C ₂ HOH ⁺	C ₂ N ₂ ⁺	C ₂ O ⁺	C ₃	C ₃ ⁺	C ₃ H	C ₃ H ⁺	C ₃ H ₂
C ₃ H ₂ ⁺	C ₃ H ₂ O ⁺	C ₃ H ₃	C ₃ H ₃ ⁺	C ₃ H ₄	C ₃ H ₄ ⁺	C ₃ H ₅ ⁺	C ₃ H ₆ OH ⁺	C ₃ N	C ₃ N ⁺
C ₃ O	C ₃ O ⁺	C ₄	C ₄ ⁺	C ₄ H	C ₄ H ⁺	C ₄ H ₂	C ₄ H ₂ ⁺	C ₄ H ₃ ⁺	C ₄ H ₃ ⁺
C ₄ N ⁺	CCN	CCN ⁺	CCNH ⁺	CCO	CH	CH ⁺	CH ₂	CH ₂ ⁺	CH ₂ CN
CH ₂ CN ⁺	CH ₂ CO	CH ₂ CO ⁺	CH ₂ NH	CH ₂ NH ₂ ⁺	CH ₂ OC	CH ₂ OH	CH ₂ OH ⁺	CH ₃	CH ₃ ⁺
CH ₃ CHO	CH ₃ CHO ⁺	CH ₃ CN	CH ₃ CN ⁺	CH ₃ CO ⁺	CH ₃ O	CH ₃ O ⁺	CH ₃ OC	CH ₃ OC ⁺	CH ₃ OCH
CH ₃ OCH ⁺	CH ₃ OCH ₂	CH ₃ OCH ₂ ⁺	CH ₃ OCH ₃	CH ₃ OCH ₃ ⁺	CH ₃ OH	CH ₃ OH ⁺	CH ₃ OH ₂ ⁺	CH ₄	CH ₄ ⁺
CH ₄ N ⁺	CH ₅ ⁺	CHOC	CHOH	CHOH ⁺	CHOOH	CHOOH ₂ ⁺	CN	CN ⁺	CN ⁻
CNC ⁺	CO	CO ⁺	CO ₂	CO ₂ ⁺	COC	COH	COOCH ₄ ⁺	H	H ⁺
H ⁻	H ₂	H ₂ ⁺	H ₂ C ₃	H ₂ C ₃ H ⁺	H ₂ C ₃ N ⁺	H ₂ C ₄ N ⁺	H ₂ CN	H ₂ CO	H ₂ CO ⁺
H ₂ NC ⁺	H ₂ NO ⁺	H ₂ O	H ₂ O ⁺	H ₂ O ₂	H ₃ ⁺	H ₃ C ₃ N	H ₃ C ₃ O ⁺	H ₃ C ₄ N	H ₃ C ₄ N ⁺
H ₃ CO ⁺	H ₃ O ⁺	H ₄ C ₂ N ⁺	H ₄ C ₃ N ⁺	H ₄ C ₄ N ⁺	H ₅ C ₂ O ⁺	H ₅ C ₂ O ₂ ⁺	HC ₂ O ⁺	HC ₃ N	HC ₃ N ⁺
HC ₃ O ⁺	HC ₄ N ⁺	HCN	HCN ⁺	HCNH ⁺	HCO	HCO ⁺	HCO ₂ ⁺	HCOOCH ₃	He
He ⁺	HeH ⁺	HNC	HNCO ⁺	HNO	HNO ⁺	HOC ⁺	Mg	Mg ⁺	N
N ⁺	N ₂	N ₂ ⁺	N ₂ H ⁺	N ₂ O	NCO ⁺	NH	NH ⁺	NH ₂	NH ₂ ⁺
NH ₃	NH ₃ ⁺	NH ₄ ⁺	NO	NO ⁺	NO ₂	NO ₂ ⁺	O	O ⁺	O ⁻
O ₂	O ₂ ⁺	O ₂ H	O ₂ H ⁺	OCN	OH	OH ⁺	OH ⁻	ELECTR	

Table 18. Solid phase reactions used for complex molecule formation

	Reactant1	Reactant2	Product1	Product2	Activation Energy E_a (K)
1	*C	*CO	*CCO		5.0×10^2
2	*C	*CO	*COC		5.0×10^2
3	*C	*H	*CH		0.0
4	*C	*N	*CN		0.0
5	*C	*NH	*HNC		0.0
6	*C	*NH ₂	*H	*HNC	0.0
7	*C	*O	*CO		0.0
8	*C	*O ₂	*CO	*O	0.0
9	*C	*OH	*CO	*H	0.0
10	*C	*OH	*COH		0.0
11	*C ₂ H ₃ O	*H	*CH ₃ CHO		0.0
12	*C ₂ H ₅ O	*H	*C ₂ H ₅ OH		0.0
13	*C ₂ HO	*H	*CH ₂ CO		0.0
14	*CCO	*H	*C ₂ HO		0.0
15	*CH	*H	*CH ₂		0.0
16	*CH	*O	*HCO		0.0
17	*CH	*OH	*CHOH		0.0
18	*CH ₂	*H	*CH ₃		0.0
19	*CH ₂	*O	*H ₂ CO		0.0
20	*CH ₂	*OH	*CH ₂ OH		0.0
21	*CH ₂ CO	*H	*C ₂ H ₃ O		0.0
22	*CH ₂ OC	*H	*CH ₃ OC		0.0
23	*CH ₂ OH	*H	*CH ₃ OH		0.0
24	*CH ₃	*H	*CH ₄		0.0
25	*CH ₃	*O	*CH ₃ O		0.0
26	*CH ₃	*OH	*CH ₃ OH		0.0
27	*CH ₃ CHO	*H	*C ₂ H ₅ O		0.0
28	*CH ₃ O	*H	*CH ₃ OH		0.0
29	*CH ₃ OC	*H	*CH ₃ OCH		0.0
30	*CH ₃ OCH	*H	*CH ₃ OCH ₂		0.0
31	*CH ₃ OCH ₂	*H	*CH ₃ OCH ₃		0.0
32	*CHOC	*H	*CH ₂ OC		0.0
33	*CHOH	*H	*CH ₂ OH		0.0
34	*CN	*H	*HCN		0.0
35	*CO	*H	*COH		3.0×10^3
36	*CO	*H	*HCO		1.0×10^3
37	*CO	*OH	*CO ₂	*H	3.0×10^2
38	*COC	*H	*CHOC		0.0
39	*COH	*H	*CHOH		0.0
40	*H	*H	*H ₂		0.0
41	*H	*H ₂ CO	*H ₂	*HCO	1.85×10^3
42	*H	*HCO	*CO	*H ₂	0.0
43	*H	*N	*NH		0.0
44	*H	*NH	*NH ₂		0.0
45	*H	*NH ₂	*NH ₃		0.0
46	*H	*NO	*HNO		0.0
47	*H	*O	*OH		0.0
48	*H	*OH	*H ₂ O		0.0
49	*HCO	*O	*CO	*OH	0.0
50	*HCO	*O	*CO ₂	*H	2.0×10^1
51	*N	*O	*NO		0.0
52	*N	*OH	*HNO		0.0
53	*NH	*O	*HNO		0.0
54	*O	*O	*O ₂		0.0

Table 18. Gas phase reactions used for complex molecule destruction

	Reactant1	Reactant2	Product1	Product2	Product3	Product4	α	β	γ
1	C ⁺	C ₂ H ₃ O	C ₂ H ₃ ⁺	CO			1.50×10^{-09}	0.00	0.0
2	C ⁺	C ₂ H ₅ O	C ₂ H ₅ ⁺	CO			1.50×10^{-09}	0.00	0.0
3	C ⁺	C ₂ HO	C ₂ H ⁺	CO			1.50×10^{-09}	0.00	0.0
4	C ⁺	CH ₂ OC	C ₂ H ⁺	HCO			1.50×10^{-09}	0.00	0.0
5	C ⁺	CH ₂ OH	CH ₃ ⁺	CO			1.50×10^{-09}	0.00	0.0
6	C ⁺	CH ₃ O	CH ₃ ⁺	CO			1.50×10^{-09}	0.00	0.0
7	C ⁺	CH ₃ OC	C	CH ₃ ⁺	CO		1.50×10^{-09}	0.00	0.0
8	C ⁺	CH ₃ OCH	CH	CH ₃ ⁺	CO		1.50×10^{-09}	0.00	0.0
9	C ⁺	CH ₃ OCH ₂	CH ₂	CH ₃ ⁺	CO		1.50×10^{-09}	0.00	0.0
10	C ⁺	CHOC	C ₂ H ⁺	CO			1.50×10^{-09}	0.00	0.0
11	C ⁺	CHOH	C	CHOH ⁺			7.80×10^{-10}	0.00	0.0
12	C ⁺	CHOH	CH	HCO ⁺			7.80×10^{-10}	0.00	0.0
13	C ⁺	CHOH	CH ₂ ⁺	CO			2.34×10^{-09}	0.00	0.0
14	C ⁺	COC	C ₂ ⁺	CO			1.50×10^{-09}	0.00	0.0
15	C ⁺	COH	C ₂ ⁺	OH			1.50×10^{-09}	0.00	0.0
16	C ₂ H ₃ O	CRPHOT	C ₂ H ₂	OH			1.30×10^{-17}	0.00	4307.0
17	C ₂ H ₃ O	H ⁺	C ₂ H ₃ O ⁺	H			3.00×10^{-09}	0.00	0.0
18	C ₂ H ₃ O	H ₃ ⁺	C ₂ H ₄ O ⁺	H ₂			4.85×10^{-09}	0.00	0.0
19	C ₂ H ₃ O	HCO ⁺	C ₂ H ₄ O ⁺	CO			2.20×10^{-09}	0.00	0.0
20	C ₂ H ₃ O	He ⁺	C ₂ H ₂ ⁺	He	OH		3.00×10^{-09}	0.00	0.0
21	C ₂ H ₃ O	O	CH ₃	CO ₂			1.60×10^{-11}	0.00	0.0
22	C ₂ H ₃ O ⁺	ELECTR	C ₂ H ₂	OH			1.50×10^{-07}	-0.50	0.0
23	C ₂ H ₄ O ⁺	ELECTR	C ₂ H ₂	H ₂ O			1.50×10^{-07}	-0.50	0.0
24	C ₂ H ₅ O	CRPHOT	C ₂ H ₄	OH			1.30×10^{-17}	0.00	4307.0
25	C ₂ H ₅ O	H ⁺	C ₂ H ₅ O ⁺	H			3.00×10^{-09}	0.00	0.0
26	C ₂ H ₅ O	H ₃ ⁺	C ₂ H ₆ O ⁺	H ₂			4.85×10^{-09}	0.00	0.0
27	C ₂ H ₅ O	HCO ⁺	C ₂ H ₆ O ⁺	CO			2.20×10^{-09}	0.00	0.0
28	C ₂ H ₅ O	He ⁺	C ₂ H ₄ ⁺	He	OH		3.00×10^{-09}	0.00	0.0
29	C ₂ H ₅ O	O	CH ₄	CO ₂	H		1.50×10^{-10}	0.00	0.0
30	C ₂ HO	CRPHOT	C ₂	OH			1.30×10^{-17}	0.00	4307.0
31	C ₂ HO	H ⁺	C ₂ HO ⁺	H			3.00×10^{-09}	0.00	0.0
32	C ₂ HO	H ₃ ⁺	C ₂ HOH ⁺	H ₂			4.85×10^{-09}	0.00	0.0
33	C ₂ HO	HCO ⁺	C ₂ HOH ⁺	CO			2.20×10^{-09}	0.00	0.0
34	C ₂ HO	He ⁺	C ₂ ⁺	He	OH		3.00×10^{-09}	0.00	0.0
35	C ₂ HO	O	CO	CO	H		1.60×10^{-10}	0.00	0.0
36	C ₂ HOH ⁺	ELECTR	C ₂ H	OH			1.50×10^{-07}	-0.50	0.0
37	CH ₂ OC	CRPHOT	CH ₂	CO			1.30×10^{-17}	0.00	4307.0
38	CH ₂ OC	H ⁺	CH ₂	HCO ⁺			3.00×10^{-09}	0.00	0.0
39	CH ₂ OC	H ₃ ⁺	CH ₄	HCO ⁺			4.85×10^{-09}	0.00	0.0
40	CH ₂ OC	HCO ⁺	CH ₃	CO	CO ⁺		2.20×10^{-09}	0.00	0.0
41	CH ₂ OC	He ⁺	CH ₂ ⁺	CO	He		3.00×10^{-09}	0.00	0.0
42	CH ₂ OC	O	CH ₂	CO ₂			1.60×10^{-10}	0.00	0.0
43	CH ₂ OH	CRPHOT	CH ₂	OH			1.30×10^{-17}	0.00	4307.0
44	CH ₂ OH	H ⁺	CH ₂ OH ⁺	H			3.00×10^{-09}	0.00	0.0
45	CH ₂ OH	H ₃ ⁺	CH ₃ OH ⁺	H ₂			4.85×10^{-09}	0.00	0.0
46	CH ₂ OH	HCO ⁺	CH ₃ OH ⁺	CO			2.20×10^{-09}	0.00	0.0
47	CH ₂ OH	He ⁺	CH ₂ ⁺	He	OH		3.00×10^{-09}	0.00	0.0
48	CH ₂ OH	O	CH ₃	O ₂			1.50×10^{-11}	0.00	0.0
49	CH ₂ OH	O	H ₂ CO	OH			1.00×10^{-11}	0.00	0.0
50	CH ₂ OH ⁺	ELECTR	CH ₂	OH			1.50×10^{-07}	-0.50	0.0
51	CH ₃ O	CRPHOT	CH ₃	O			1.30×10^{-17}	0.00	4307.0
52	CH ₃ O	H ⁺	CH ₃ O ⁺	H			3.00×10^{-09}	0.00	0.0
53	CH ₃ O	H ₃ ⁺	CH ₃ OH ⁺	H ₂			4.85×10^{-09}	0.00	0.0
54	CH ₃ O	HCO ⁺	CH ₃ OH ⁺	CO			2.20×10^{-09}	0.00	0.0
55	CH ₃ O	He ⁺	CH ₃ ⁺	He	O		3.00×10^{-09}	0.00	0.0
56	CH ₃ O	O	CH ₃	O ₂			1.50×10^{-11}	0.00	0.0
57	CH ₃ O	O	H ₂ CO	OH			1.00×10^{-11}	0.00	0.0
58	CH ₃ O ⁺	ELECTR	CH ₃	O			1.50×10^{-07}	-0.50	0.0
59	CH ₃ OC	CRPHOT	CH ₃	CO			1.30×10^{-17}	0.00	4307.0
60	CH ₃ OC	H ⁺	CH ₃ OC ⁺	H			3.00×10^{-09}	0.00	0.0
61	CH ₃ OC	H ₃ ⁺	CH ₃ OCH ⁺	H ₂			4.85×10^{-09}	0.00	0.0
62	CH ₃ OC	HCO ⁺	CH ₃ OCH ⁺	CO			2.20×10^{-09}	0.00	0.0
63	CH ₃ OC	He ⁺	CH ₃ ⁺	CO	He		3.00×10^{-09}	0.00	0.0
64	CH ₃ OC	O	CH ₃ O	CO			1.00×10^{-11}	0.00	0.0

Table 18. Gas phase reactions used for complex molecule destruction - continued

	Reactant1	Reactant2	Product1	Product2	Product3	Product4	α	β	γ
65	CH ₃ OC ⁺	ELECTR	CH ₃	CO			1.50×10^{-07}	-0.50	0.0
66	CH ₃ OCH	CRPHOT	CH ₃	HCO			1.30×10^{-17}	0.00	4307.0
67	CH ₃ OCH	H ⁺	CH ₃ OCH ⁺	H			3.00×10^{-09}	0.00	0.0
68	CH ₃ OCH	H ₃ ⁺	CH ₃ OCH ₂ ⁺	H ₂			4.85×10^{-09}	0.00	0.0
69	CH ₃ OCH	HCO ⁺	CH ₃ OCH ₂ ⁺	CO			2.20×10^{-09}	0.00	0.0
70	CH ₃ OCH	He ⁺	CH ₄ ⁺	CO	He		3.00×10^{-09}	0.00	0.0
71	CH ₃ OCH	O	CH ₃ O	CO	H		1.00×10^{-11}	0.00	0.0
72	CH ₃ OCH ⁺	ELECTR	CH ₃	CO	H		1.50×10^{-07}	-0.50	0.0
73	CH ₃ OCH ₂	CRPHOT	CH ₃	H ₂ CO			1.30×10^{-17}	0.00	4307.0
74	CH ₃ OCH ₂	H ⁺	CH ₃ OCH ₂ ⁺	H			3.00×10^{-09}	0.00	0.0
75	CH ₃ OCH ₂	H ₃ ⁺	CH ₃ OCH ₃ ⁺	H ₂			4.85×10^{-09}	0.00	0.0
76	CH ₃ OCH ₂	HCO ⁺	CH ₃ OCH ₃ ⁺	CO			2.20×10^{-09}	0.00	0.0
77	CH ₃ OCH ₂	He ⁺	CH ₃ ⁺	CO	H ₂	He	3.00×10^{-09}	0.00	0.0
78	CH ₃ OCH ₂	O	CH ₃ O	H ₂ CO			1.00×10^{-11}	0.00	0.0
79	CH ₃ OCH ₂ ⁺	ELECTR	CH ₃	H ₂ CO			1.50×10^{-07}	-0.50	0.0
80	CH ₃ OCH ₃ ⁺	ELECTR	CH ₃	CH ₃ O			1.50×10^{-07}	-0.50	0.0
81	CHOC	CRPHOT	CH	CO			1.30×10^{-17}	0.00	4307.0
82	CHOC	H ⁺	CH ₂	CO ⁺			3.00×10^{-09}	0.00	0.0
83	CHOC	H ₃ ⁺	CH ₃	HCO ⁺			4.85×10^{-09}	0.00	0.0
84	CHOC	HCO ⁺	CH ₂	CO	CO ⁺		2.20×10^{-09}	0.00	0.0
85	CHOC	He ⁺	CH ⁺	CO	He		3.00×10^{-09}	0.00	0.0
86	CHOC	O	CH	CO ₂			1.60×10^{-10}	0.00	0.0
87	CHOH	CRPHOT	CO	H ₂			1.30×10^{-17}	0.00	2659.0
88	CHOH	H ⁺	CHOH ⁺	H			2.96×10^{-09}	0.00	0.0
89	CHOH	H ⁺	CO ⁺	H	H ₂		1.06×10^{-09}	0.00	0.0
90	CHOH	H ⁺	H ₂	HCO ⁺			3.57×10^{-09}	0.00	0.0
91	CHOH	H ₃ ⁺	H ₂	H ₃ CO ⁺			6.30×10^{-09}	0.00	0.0
92	CHOH	HCO ⁺	CO	H ₃ CO ⁺			3.30×10^{-09}	0.00	0.0
93	CHOH	He ⁺	CH ₂ ⁺	He	O		1.71×10^{-09}	0.00	0.0
94	CHOH	He ⁺	CHOH ⁺	He			9.69×10^{-10}	0.00	0.0
95	CHOH	He ⁺	CO ⁺	H ₂	He		1.88×10^{-09}	0.00	0.0
96	CHOH	He ⁺	H	HCO ⁺	He		1.14×10^{-09}	0.00	0.0
97	CHOH	O	HCO	OH			1.78×10^{-11}	0.57	1390.0
98	CHOH ⁺	ELECTR	CO	H	H		5.00×10^{-07}	-0.50	0.0
99	CHOH ⁺	ELECTR	H	HCO			1.00×10^{-07}	-0.50	0.0
100	CHOH ⁺	ELECTR	H ₂ CO	PHOTON			1.10×10^{-10}	-0.70	0.0
101	COC	CRPHOT	C	CO			1.30×10^{-17}	0.00	4307.0
102	COC	H ⁺	CH	CO ⁺			3.00×10^{-09}	0.00	0.0
103	COC	H ₃ ⁺	CH ₃	CO ⁺			4.85×10^{-09}	0.00	0.0
104	COC	HCO ⁺	CH	CO	CO ⁺		2.20×10^{-09}	0.00	0.0
105	COC	He ⁺	C ⁺	CO	He		3.00×10^{-09}	0.00	0.0
106	COC	O	CO	CO			1.60×10^{-10}	0.00	0.0
107	COH	CRPHOT	C	OH			1.30×10^{-17}	0.00	4307.0
108	COH	H ⁺	CH	OH ⁺			3.00×10^{-09}	0.00	0.0
109	COH	H ₃ ⁺	CH ₃	OH ⁺			4.85×10^{-09}	0.00	0.0
110	COH	HCO ⁺	CH	CO ⁺	OH		2.20×10^{-09}	0.00	0.0
111	COH	He ⁺	C ⁺	He	OH		3.00×10^{-09}	0.00	0.0
112	COH	O	CO	OH			1.60×10^{-10}	0.00	0.0

Table 19. Model 1 - Free fall collapse from 100 cm^{-3} - most abundant gas phase species

Plateau Point 4.389×10^6 years			Plateau Point + 2.0×10^5 years 4.589×10^6 years		
	Species	Abundance (w.r.t H + H ₂)		Species	Abundance (w.r.t H + H ₂)
1	H ₂	5.000×10^{-01}	1	H ₂	5.000×10^{-01}
2	He	1.401×10^{-01}	2	He	1.401×10^{-01}
3	H ₂ O	1.554×10^{-04}	3	H ₂ O	1.447×10^{-04}
4	CH ₄	5.260×10^{-05}	4	CH ₄	3.980×10^{-05}
5	CH ₃ OH	1.116×10^{-05}	5	CO ₂	1.462×10^{-05}
6	NH ₃	8.369×10^{-06}	6	N ₂	7.593×10^{-06}
7	N ₂	6.114×10^{-06}	7	HCN	2.847×10^{-06}
8	CO	4.929×10^{-06}	8	HNC	1.607×10^{-06}
9	CO ₂	1.352×10^{-06}	9	C ₄ H	8.936×10^{-07}
10	NH ₂	3.999×10^{-07}	10	CH ₂ CN	8.380×10^{-07}
11	CH ₃	3.254×10^{-07}	11	CH ₃ OCH ₃	8.361×10^{-07}
12	CH ₃ OCH ₃	3.006×10^{-07}	12	C ₃ H ₃	6.461×10^{-07}
13	H ₂ CO	2.946×10^{-07}	13	HC ₃ N	5.801×10^{-07}
14	O ₂	2.416×10^{-07}	14	CH ₃ OH	4.315×10^{-07}
15	HCN	1.916×10^{-07}	15	C ₃ H	3.657×10^{-07}
16	C ₄ H	1.545×10^{-07}	16	C ₂	2.372×10^{-07}
17	HNC	1.193×10^{-07}	17	CH ₃ CN	1.923×10^{-07}
18	C ₃ H	8.901×10^{-08}	18	C ₄ H ₂	6.160×10^{-08}
19	CH	4.796×10^{-08}	19	CH	5.320×10^{-08}
20	NH	2.391×10^{-08}	20	C ₃ H ₂	5.081×10^{-08}
21	C ₃ H ₃	1.873×10^{-08}	21	C ₃ N	3.511×10^{-08}
22	H	1.364×10^{-08}	22	C ₃	3.456×10^{-08}
23	CH ₂	9.769×10^{-09}	23	CH ₃	2.655×10^{-08}
24	C ₂ H ₄	8.988×10^{-09}	24	CCN	2.442×10^{-08}

Table 20. Model 2 - Free fall collapse from $1,000 \text{ cm}^{-3}$ - most abundant gas phase species

Plateau Point 1.388×10^6 years			Plateau Point + 2.0×10^5 years 1.588×10^6 years		
	Species	Abundance (w.r.t H + H ₂)		Species	Abundance (w.r.t H + H ₂)
1	H ₂	5.000×10^{-01}	1	H ₂	5.000×10^{-01}
2	He	1.401×10^{-01}	2	He	1.401×10^{-01}
3	H ₂ O	1.375×10^{-04}	3	H ₂ O	1.300×10^{-04}
4	CH ₄	3.880×10^{-05}	4	CH ₄	3.118×10^{-05}
5	CH ₃ OH	1.834×10^{-05}	5	CO ₂	2.121×10^{-05}
6	CO	8.797×10^{-06}	6	N ₂	8.945×10^{-06}
7	N ₂	8.063×10^{-06}	7	CH ₃	3.178×10^{-06}
8	NH ₃	4.633×10^{-06}	8	H ₂ CO	1.768×10^{-06}
9	CO ₂	3.475×10^{-06}	9	C ₄ H	1.450×10^{-06}
10	O ₂	1.413×10^{-06}	10	HCN	1.444×10^{-06}
11	CH ₃	4.982×10^{-07}	11	HNC	1.382×10^{-06}
12	H ₂ CO	4.366×10^{-07}	12	CH ₃ OCH ₃	5.813×10^{-07}
13	CH ₃ OCH ₃	4.110×10^{-07}	13	C ₂	4.082×10^{-07}
14	NH ₂	3.131×10^{-07}	14	CH ₃ OH	3.799×10^{-07}
15	C ₄ H	2.115×10^{-07}	15	C ₃ H	3.768×10^{-07}
16	HCN	1.361×10^{-07}	16	CH ₂ CN	3.276×10^{-07}
17	HNC	8.830×10^{-08}	17	C ₃ H ₃	2.841×10^{-07}
18	C ₃ H	7.771×10^{-08}	18	HC ₃ N	2.025×10^{-07}
19	CH	3.446×10^{-08}	19	C ₃ H ₂	8.748×10^{-08}
20	NH	2.147×10^{-08}	20	C ₃	8.348×10^{-08}
21	C ₂ H ₄	1.672×10^{-08}	21	CH	6.791×10^{-08}
22	H	1.329×10^{-08}	22	C ₄ H ₂	6.266×10^{-08}
23	C ₂ H ₂	1.205×10^{-08}	23	CO	4.991×10^{-08}
24	OCN	1.130×10^{-08}	24	C ₂ H ₅ OH	3.318×10^{-08}

Table 21. Model 3 - Free fall collapse from $10,000 \text{ cm}^{-3}$ - most abundant gas phase species

Plateau Point 4.381×10^5 years			Plateau Point + 2.0×10^5 years 6.381×10^5 years		
	Species	Abundance (w.r.t H + H ₂)		Species	Abundance (w.r.t H + H ₂)
1	H ₂	5.000×10^{-01}	1	H ₂	5.000×10^{-01}
2	He	1.401×10^{-01}	2	He	1.401×10^{-01}
3	H ₂ O	1.494×10^{-04}	3	H ₂ O	1.403×10^{-04}
4	CH ₄	4.801×10^{-05}	4	CH ₄	3.849×10^{-05}
5	CH ₃ OH	1.555×10^{-05}	5	CO ₂	1.667×10^{-05}
6	N ₂	6.961×10^{-06}	6	N ₂	8.063×10^{-06}
7	NH ₃	6.807×10^{-06}	7	HCN	2.385×10^{-06}
8	CO	4.811×10^{-06}	8	HNC	1.355×10^{-06}
9	CO ₂	1.700×10^{-06}	9	CH ₃ OCH ₃	1.038×10^{-06}
10	O ₂	6.601×10^{-07}	10	C ₄ H	8.916×10^{-07}
11	CH ₃	4.107×10^{-07}	11	CH ₂ CN	6.885×10^{-07}
12	H ₂ CO	3.875×10^{-07}	12	C ₃ H ₃	5.968×10^{-07}
13	CH ₃ OCH ₃	3.630×10^{-07}	13	HC ₃ N	5.436×10^{-07}
14	NH ₂	3.204×10^{-07}	14	CH ₃ OH	5.232×10^{-07}
15	HCN	1.606×10^{-07}	15	C ₃ H	3.802×10^{-07}
16	C ₄ H	1.090×10^{-07}	16	C ₂	2.579×10^{-07}
17	HNC	8.841×10^{-08}	17	CH ₃ CN	1.528×10^{-07}
18	C ₃ H	6.344×10^{-08}	18	C ₄ H ₂	6.469×10^{-08}
19	CH	4.268×10^{-08}	19	C ₃ H ₂	5.613×10^{-08}
20	NH	2.196×10^{-08}	20	CH	5.452×10^{-08}
21	OCN	1.872×10^{-08}	21	C ₃	3.771×10^{-08}
22	C ₃ H ₃	1.502×10^{-08}	22	CH ₃	3.374×10^{-08}
23	H	1.335×10^{-08}	23	C ₃ N	3.340×10^{-08}
24	C ₂ H ₄	1.332×10^{-08}	24	H ₂ CO	2.230×10^{-08}

Table 22. Model 4 - Retarded collapse from 100 cm^{-3} - most abundant gas phase species

Plateau Point 2.193×10^7 years			Plateau Point + 2.0×10^5 years 2.213×10^7 years		
	Species	Abundance (w.r.t H + H ₂)		Species	Abundance (w.r.t H + H ₂)
1	H ₂	5.000×10^{-01}	1	H ₂	5.000×10^{-01}
2	He	1.401×10^{-01}	2	He	1.400×10^{-01}
3	H ₂ O	1.158×10^{-04}	3	H ₂ O	1.021×10^{-04}
4	CH ₄	3.190×10^{-05}	4	CO ₂	2.822×10^{-05}
5	CO	1.416×10^{-05}	5	CH ₄	2.185×10^{-05}
6	CO ₂	1.155×10^{-05}	6	CO	1.184×10^{-05}
7	N ₂	1.033×10^{-05}	7	N ₂	1.034×10^{-05}
8	CH ₃ OH	8.562×10^{-06}	8	H ₂ CO	4.623×10^{-06}
9	O ₂	5.938×10^{-06}	9	C ₄ H	9.170×10^{-07}
10	CH ₃ OCH ₃	8.609×10^{-07}	10	HCN	2.600×10^{-07}
11	H ₂ CO	8.562×10^{-07}	11	HNC	2.474×10^{-07}
12	CH ₃	6.489×10^{-07}	12	C ₃ H	1.636×10^{-07}
13	C ₄ H	5.230×10^{-07}	13	C ₃ H ₃	1.141×10^{-07}
14	NH ₃	2.774×10^{-07}	14	CH ₃ OH	7.979×10^{-08}
15	C ₃ H	1.241×10^{-07}	15	C ₃ H ₂	7.747×10^{-08}
16	HCN	1.232×10^{-07}	16	CH ₃ OCH ₃	6.864×10^{-08}
17	HNC	1.008×10^{-07}	17	CH ₂ CN	6.811×10^{-08}
18	C ₂ H ₂	8.272×10^{-08}	18	C ₂ H ₅ OH	6.214×10^{-08}
19	NH ₂	7.967×10^{-08}	19	HC ₃ N	4.022×10^{-08}
20	OCN	5.908×10^{-08}	20	C ₄ H ₂	2.109×10^{-08}
21	C ₃ H ₂	4.136×10^{-08}	21	C ₂	1.836×10^{-08}
22	C ₂ H ₄	3.294×10^{-08}	22	CH	1.541×10^{-08}
23	CH	2.817×10^{-08}	23	C ₃	1.504×10^{-08}
24	C ₂	2.198×10^{-08}	24	H	1.501×10^{-08}

Table 23. Model 5 - Retarded collapse from $1,000 \text{ cm}^{-3}$ - most abundant gas phase species

Plateau Point 6.930×10^6 years			Plateau Point + 2.0×10^5 years 7.130×10^6 years		
	Species	Abundance (w.r.t H + H ₂)		Species	Abundance (w.r.t H + H ₂)
1	H ₂	5.000×10^{-01}	1	H ₂	5.000×10^{-01}
2	He	1.400×10^{-01}	2	He	1.400×10^{-01}
3	H ₂ O	6.859×10^{-05}	3	H ₂ O	4.986×10^{-05}
4	CO	4.396×10^{-05}	4	CO ₂	4.113×10^{-05}
5	CO ₂	1.946×10^{-05}	5	CO	2.959×10^{-05}
6	N ₂	1.056×10^{-05}	6	N ₂	1.064×10^{-05}
7	O ₂	8.515×10^{-06}	7	O ₂	6.551×10^{-06}
8	CH ₃ OH	5.436×10^{-06}	8	CH ₄	1.308×10^{-06}
9	CH ₃ OCH ₃	7.695×10^{-07}	9	H ₂ CO	4.522×10^{-07}
10	CH ₃	5.394×10^{-07}	10	C ₂ H ₄	6.840×10^{-08}
11	H ₂ CO	5.316×10^{-07}	11	C ₂ H ₂	2.861×10^{-08}
12	CH ₄	4.808×10^{-07}	12	O	2.465×10^{-08}
13	C ₂ H ₂	9.598×10^{-08}	13	CHOOH	1.970×10^{-08}
14	C ₄ H	6.895×10^{-08}	14	H	1.893×10^{-08}
15	HCN	4.602×10^{-08}	15	CH ₂ CN	9.355×10^{-09}
16	NH ₃	4.573×10^{-08}	16	Mg	6.969×10^{-09}
17	OCN	3.380×10^{-08}	17	C ₄ H	5.114×10^{-09}
18	HNC	3.317×10^{-08}	18	OH	3.563×10^{-09}
19	C ₃ H	2.731×10^{-08}	19	HCN	3.234×10^{-09}
20	NH ₂	2.527×10^{-08}	20	HNC	2.975×10^{-09}
21	C ₃ H ₂	2.332×10^{-08}	21	N	2.669×10^{-09}
22	H	1.423×10^{-08}	22	NH	2.406×10^{-09}
23	Mg	6.970×10^{-09}	23	NH ₃	1.498×10^{-09}
24	NH	5.941×10^{-09}	24	CH ₃ OH	1.343×10^{-09}

Table 24. Model 6 - Retarded collapse from $10,000 \text{ cm}^{-3}$ - most abundant gas phase species

Plateau Point 2.198×10^6 years			Plateau Point + 2.0×10^5 years 2.398×10^6 years		
	Species	Abundance (w.r.t H + H ₂)		Species	Abundance (w.r.t H + H ₂)
1	H ₂	5.000×10^{-01}	1	H ₂	5.000×10^{-01}
2	He	1.401×10^{-01}	2	He	1.401×10^{-01}
3	H ₂ O	1.391×10^{-04}	3	H ₂ O	1.258×10^{-04}
4	CH ₄	4.169×10^{-05}	4	CH ₄	3.347×10^{-05}
5	CH ₃ OH	1.094×10^{-05}	5	CO ₂	2.455×10^{-05}
6	N ₂	1.007×10^{-05}	6	N ₂	9.940×10^{-06}
7	CO ₂	7.513×10^{-06}	7	C ₄ H	2.133×10^{-06}
8	CO	2.971×10^{-06}	8	HCN	6.115×10^{-07}
9	H ₂ CO	1.995×10^{-06}	9	C ₃ H	4.118×10^{-07}
10	O ₂	1.747×10^{-06}	10	HNC	3.100×10^{-07}
11	CH ₃ OCH ₃	1.639×10^{-06}	11	HC ₃ N	2.558×10^{-07}
12	CH ₃	1.302×10^{-06}	12	C ₃ H ₃	2.388×10^{-07}
13	NH ₃	5.736×10^{-07}	13	C ₂	2.148×10^{-07}
14	C ₄ H	3.498×10^{-07}	14	CH ₂ CN	2.026×10^{-07}
15	HCN	2.723×10^{-07}	15	CH ₃ OCH ₃	1.920×10^{-07}
16	HNC	1.553×10^{-07}	16	CH ₃ OH	1.656×10^{-07}
17	C ₃ H	1.509×10^{-07}	17	C ₃ H ₂	9.933×10^{-08}
18	OCN	7.426×10^{-08}	18	C ₄ H ₂	9.856×10^{-08}
19	C ₃ H ₃	7.264×10^{-08}	19	C ₃	5.645×10^{-08}
20	NH ₂	6.593×10^{-08}	20	CH	5.217×10^{-08}
21	C ₃ H ₂	4.091×10^{-08}	21	C ₃ N	2.139×10^{-08}
22	CH	4.007×10^{-08}	22	CH ₃ CN	1.751×10^{-08}
23	C ₂ H ₄	3.178×10^{-08}	23	CH ₃	1.596×10^{-08}
24	C ₂	2.231×10^{-08}	24	H ₂ CO	1.518×10^{-08}

Table 25. Model 7 - Free fall collapse from $10,000 \text{ cm}^{-3}$ - H_2 starting abundance - most abundant gas phase species

Plateau Point 4.381×10^5 years			Plateau Point + 2.0×10^5 years 6.381×10^5 years		
	Species	Abundance (w.r.t H + H_2)		Species	Abundance (w.r.t H + H_2)
1	H_2	5.000×10^{-01}	1	H_2	5.000×10^{-01}
2	He	1.400×10^{-01}	2	He	1.400×10^{-01}
3	H_2O	8.079×10^{-05}	3	H_2O	5.528×10^{-05}
4	CO	3.734×10^{-05}	4	CO_2	4.766×10^{-05}
5	CO_2	2.562×10^{-05}	5	CO	2.288×10^{-05}
6	N_2	1.054×10^{-05}	6	N_2	1.064×10^{-05}
7	CH_4	2.491×10^{-06}	7	CH_4	1.801×10^{-06}
8	O_2	2.137×10^{-06}	8	O_2	8.088×10^{-07}
9	CH_3OH	8.713×10^{-07}	9	H_2CO	1.609×10^{-07}
10	C_4H	7.661×10^{-07}	10	O	2.585×10^{-08}
11	C_3H	5.091×10^{-07}	11	C_2H_2	2.445×10^{-08}
12	H_2CO	5.005×10^{-07}	12	C_4H	2.276×10^{-08}
13	CH_3OCH_3	1.936×10^{-07}	13	CHOOH	2.094×10^{-08}
14	C_2H_2	1.038×10^{-07}	14	CH_2CN	2.088×10^{-08}
15	CCN	5.875×10^{-08}	15	H	1.890×10^{-08}
16	CH_3	5.190×10^{-08}	16	C_2H_4	7.726×10^{-09}
17	HCN	4.327×10^{-08}	17	Mg	6.969×10^{-09}
18	C_3	3.276×10^{-08}	18	C_3H	4.168×10^{-09}
19	NH_3	2.411×10^{-08}	19	OH	3.816×10^{-09}
20	C_2	2.391×10^{-08}	20	CH_3OH	2.722×10^{-09}
21	C_3H_2	2.371×10^{-08}	21	N	2.559×10^{-09}
22	HNC	2.314×10^{-08}	22	NH	2.388×10^{-09}
23	$\text{C}_2\text{H}_5\text{OH}$	2.301×10^{-08}	23	NH_3	1.793×10^{-09}
24	HC_3N	1.915×10^{-08}	24	HCN	1.226×10^{-09}

Table 26. Model 8 - Retarded collapse from $10,000 \text{ cm}^{-3}$ - H_2 starting abundance - most abundant gas phase species

Plateau Point 2.198×10^6 years			Plateau Point + 2.0×10^5 years 2.398×10^6 years		
	Species	Abundance (w.r.t H + H_2)		Species	Abundance (w.r.t H + H_2)
1	H_2	5.000×10^{-01}	1	H_2	5.000×10^{-01}
2	He	1.400×10^{-01}	2	He	1.400×10^{-01}
3	H_2O	6.243×10^{-05}	3	CO_2	5.294×10^{-05}
4	CO	3.772×10^{-05}	4	H_2O	3.453×10^{-05}
5	CO_2	2.777×10^{-05}	5	CO	1.839×10^{-05}
6	N_2	1.057×10^{-05}	6	N_2	1.065×10^{-05}
7	O_2	9.298×10^{-06}	7	O_2	8.183×10^{-06}
8	CH_4	1.577×10^{-06}	8	CH_4	1.207×10^{-06}
9	C_4H	6.777×10^{-07}	9	CHOOH	5.060×10^{-08}
10	H_2CO	6.702×10^{-07}	10	O	3.969×10^{-08}
11	C_2H_2	2.364×10^{-07}	11	C_2H_4	3.818×10^{-08}
12	C_3H	2.304×10^{-07}	12	H_2CO	2.609×10^{-08}
13	CH_3OH	1.507×10^{-07}	13	H	1.888×10^{-08}
14	CH_3OCH_3	1.266×10^{-07}	14	C_2H_2	1.256×10^{-08}
15	C_3H_2	8.157×10^{-08}	15	CH_2CN	1.058×10^{-08}
16	HCN	3.963×10^{-08}	16	Mg	6.968×10^{-09}
17	CCN	3.628×10^{-08}	17	OH	3.645×10^{-09}
18	HNC	3.490×10^{-08}	18	N	3.416×10^{-09}
19	C_2	1.835×10^{-08}	19	CH_3OH	1.968×10^{-09}
20	OCN	1.683×10^{-08}	20	NH	1.784×10^{-09}
21	C_4H_2	1.657×10^{-08}	21	NH_3	1.611×10^{-09}
22	HC_3N	1.641×10^{-08}	22	NO	1.345×10^{-09}
23	H	1.619×10^{-08}	23	C_4H	5.672×10^{-10}
24	C_3	1.461×10^{-08}	24	HNO	4.566×10^{-10}

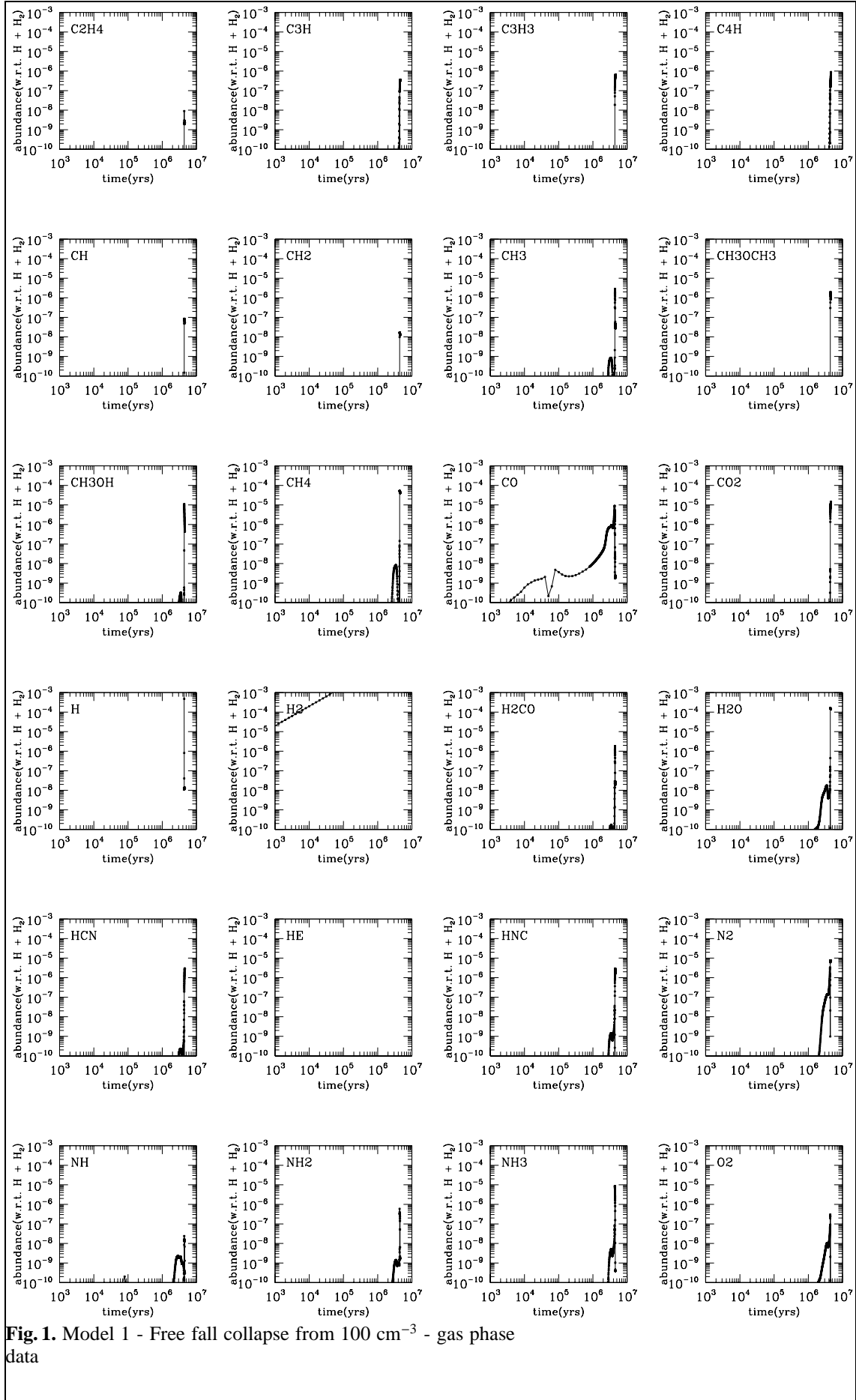


Fig. 1. Model 1 - Free fall collapse from 100 cm^{-3} - gas phase data

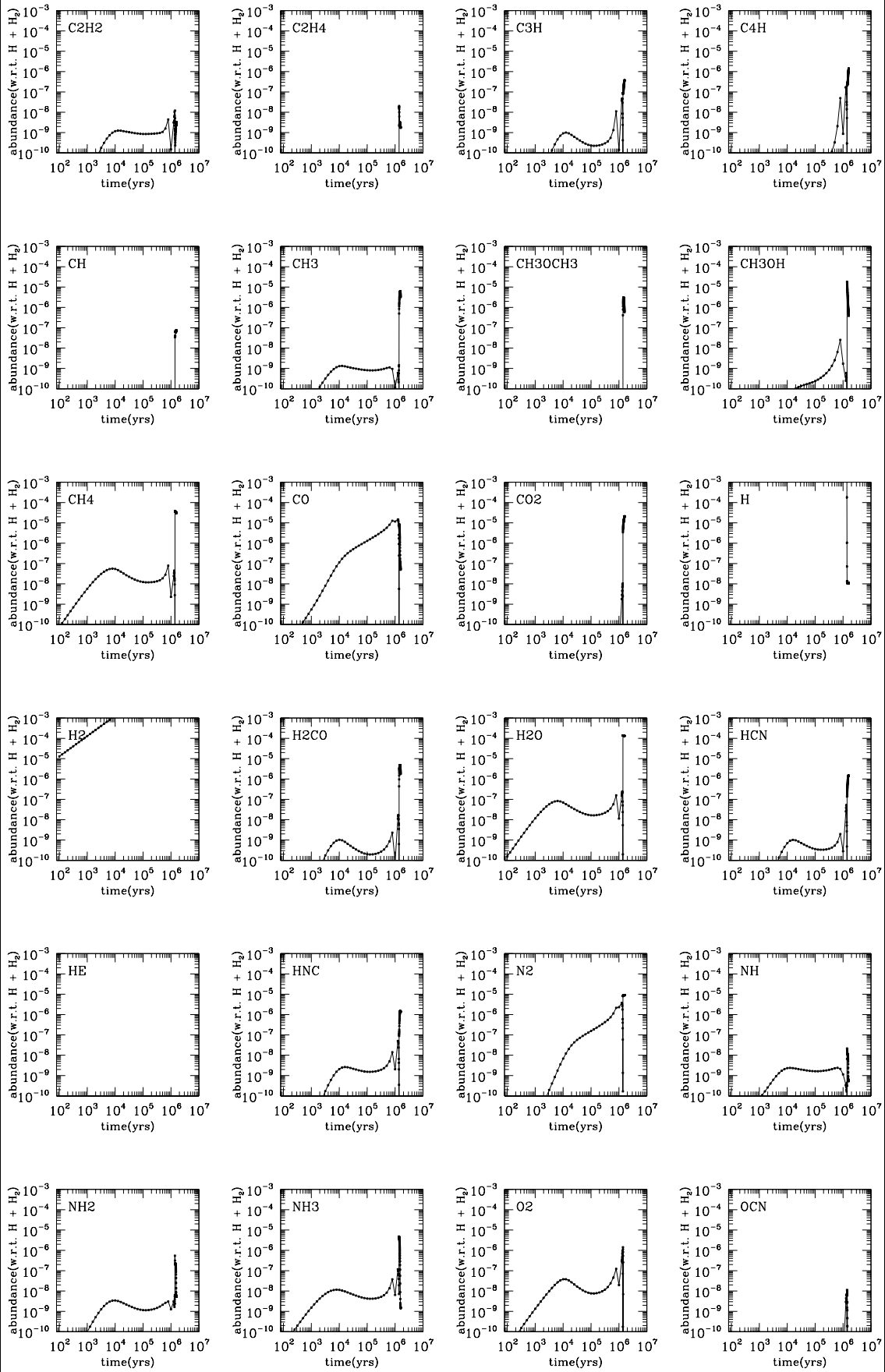


Fig. 2. Model 2 - Free fall collapse from $1,000 \text{ cm}^{-3}$ - gas phase data

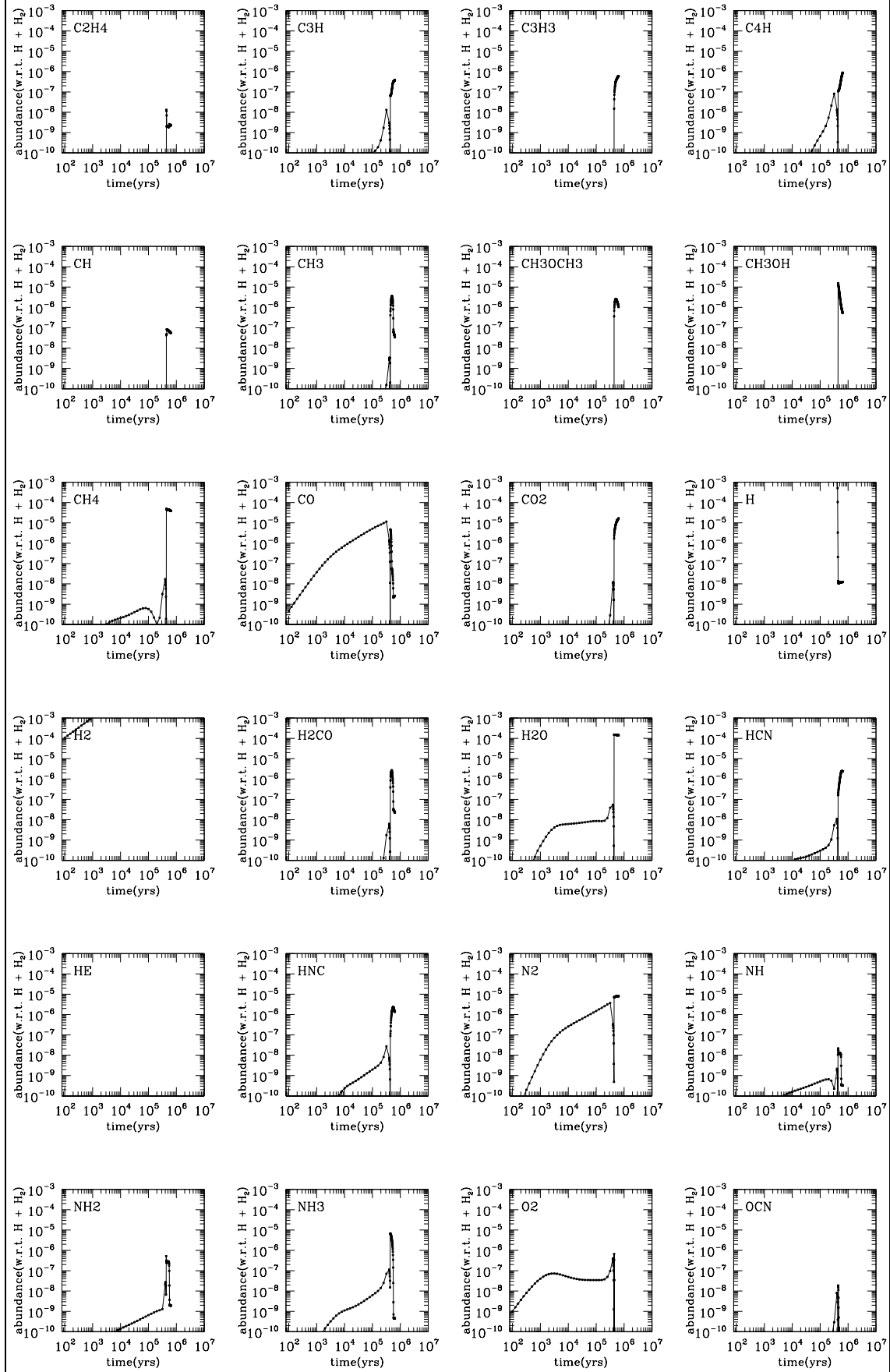


Fig. 3. Model 3 - Free fall collapse from $10,000 \text{ cm}^{-3}$ - gas phase data

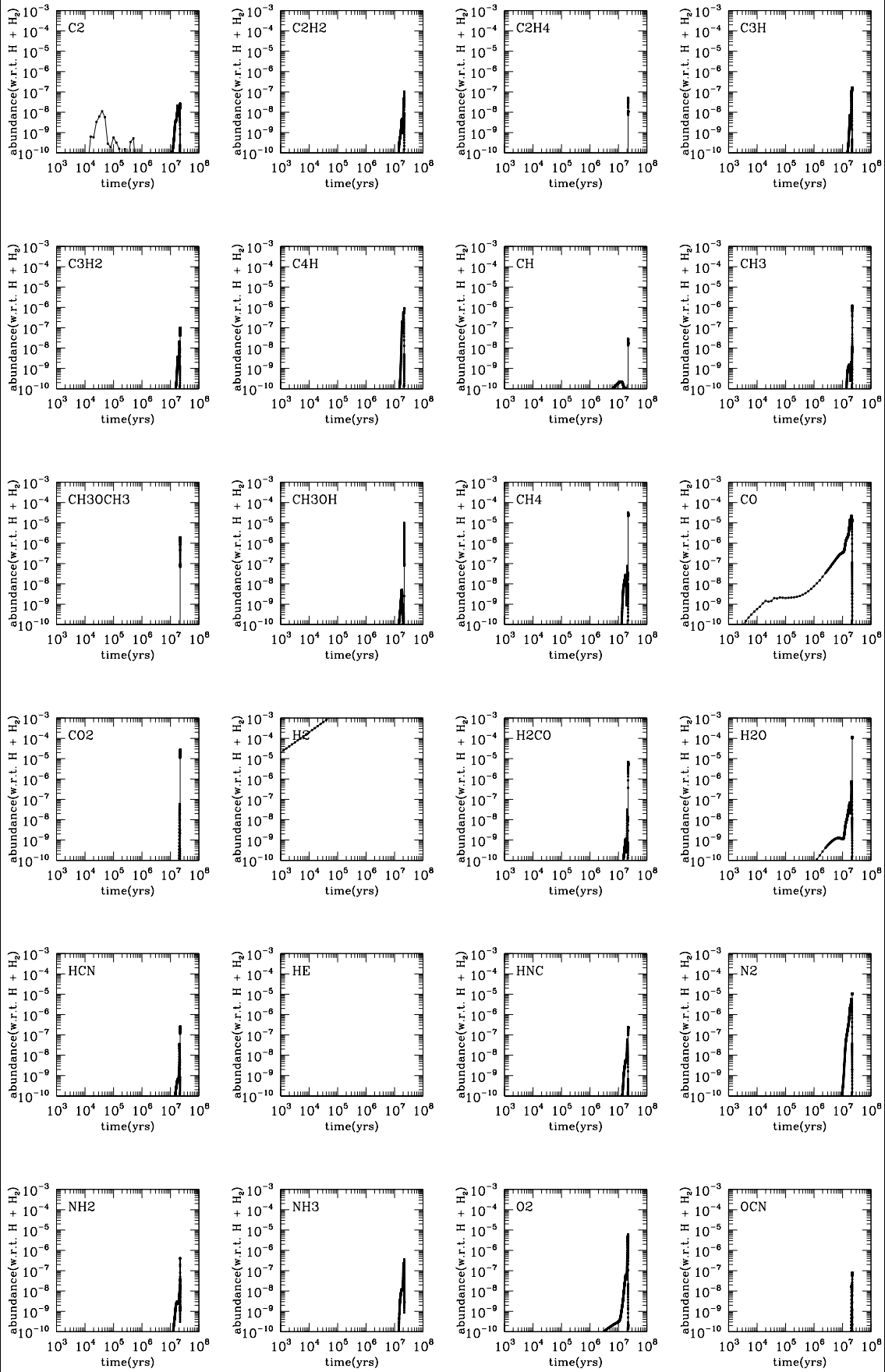


Fig. 4. Model 4 - Retarded collapse from 100 cm^{-3} - gas phase data

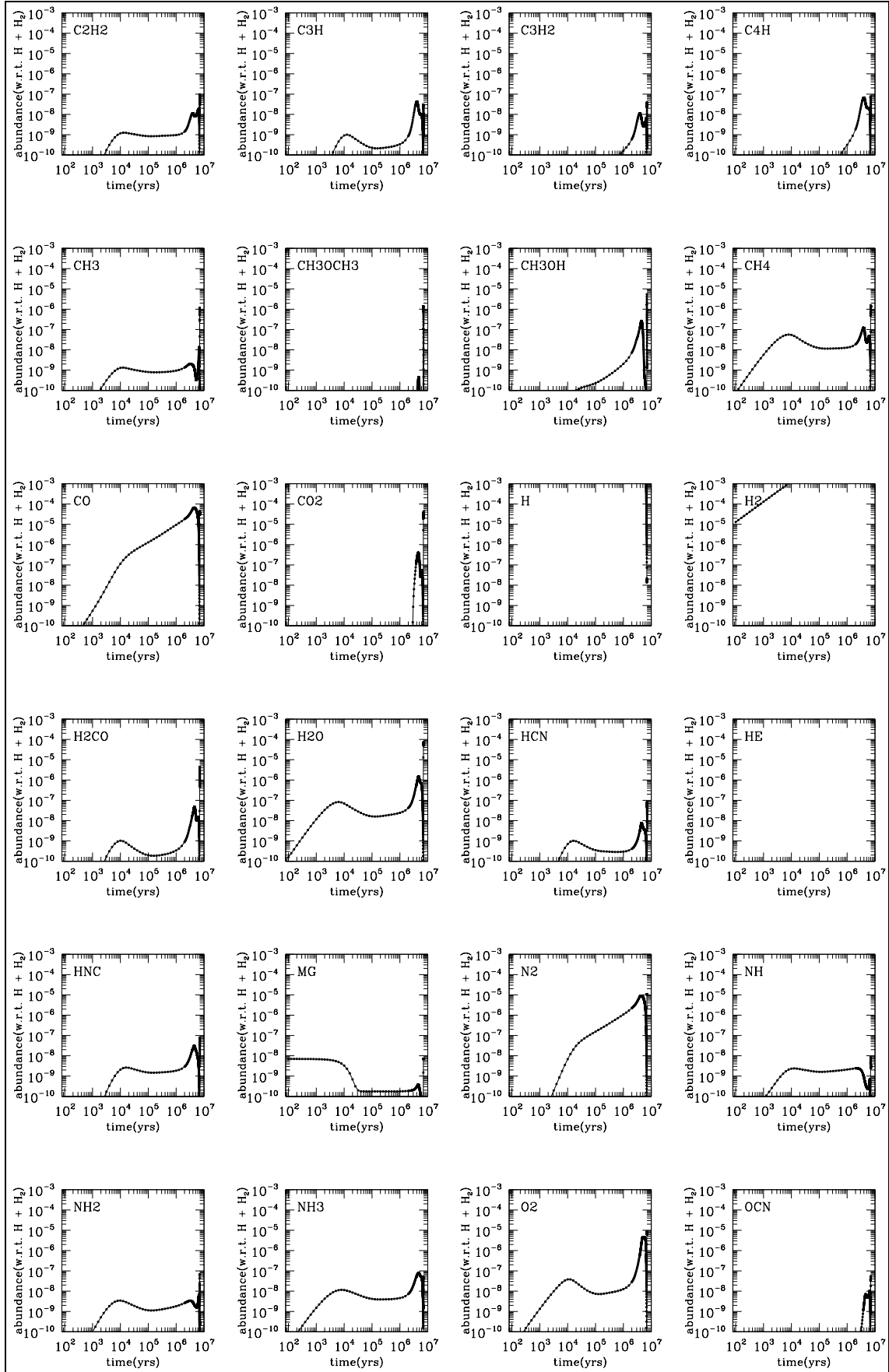


Fig. 5. Model 5 - Retarded collapse from $1,000 \text{ cm}^{-3}$ - gas phase data

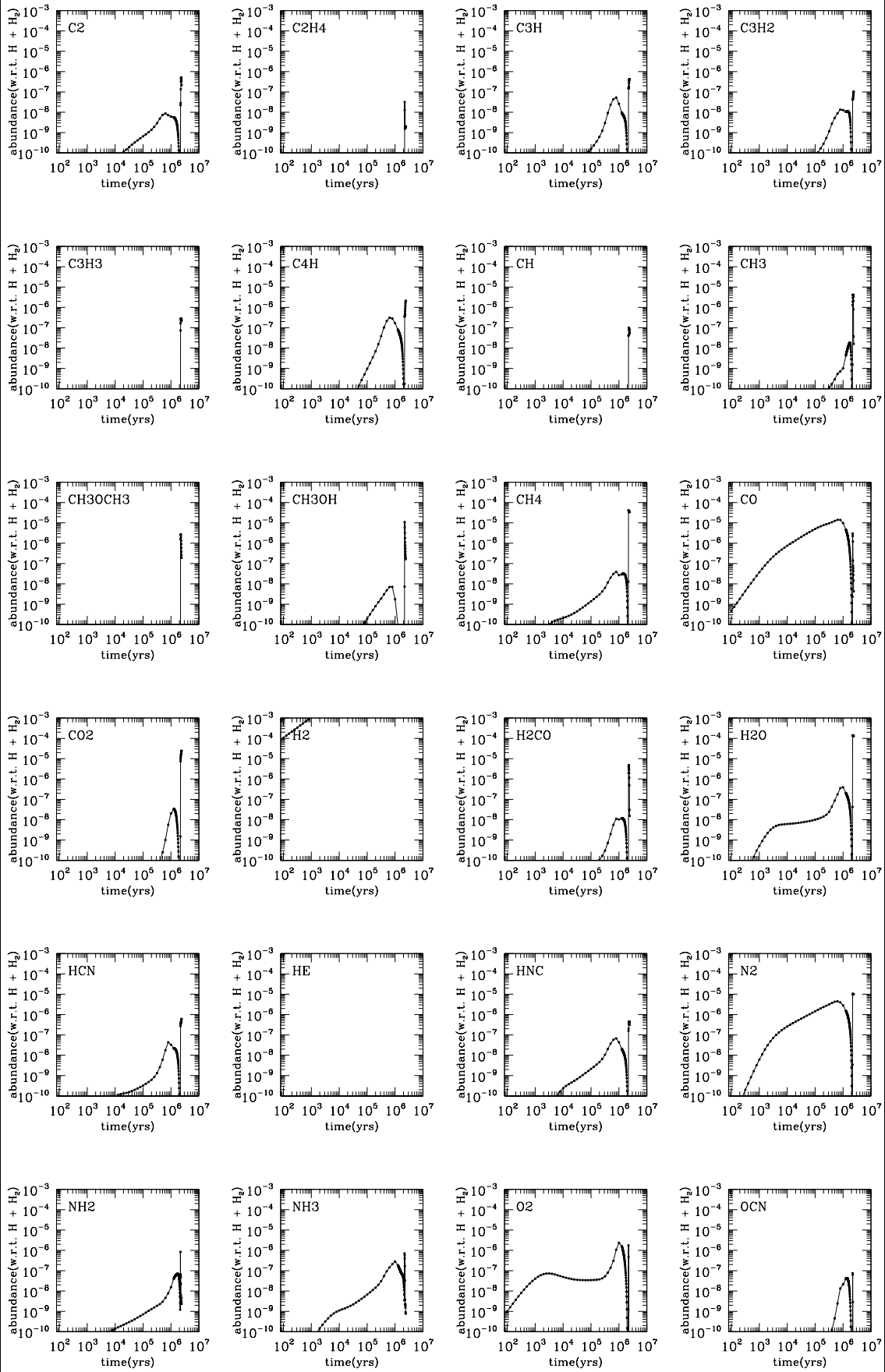


Fig. 6. Model 6 - Retarded collapse from $10,000 \text{ cm}^{-3}$ - gas phase data

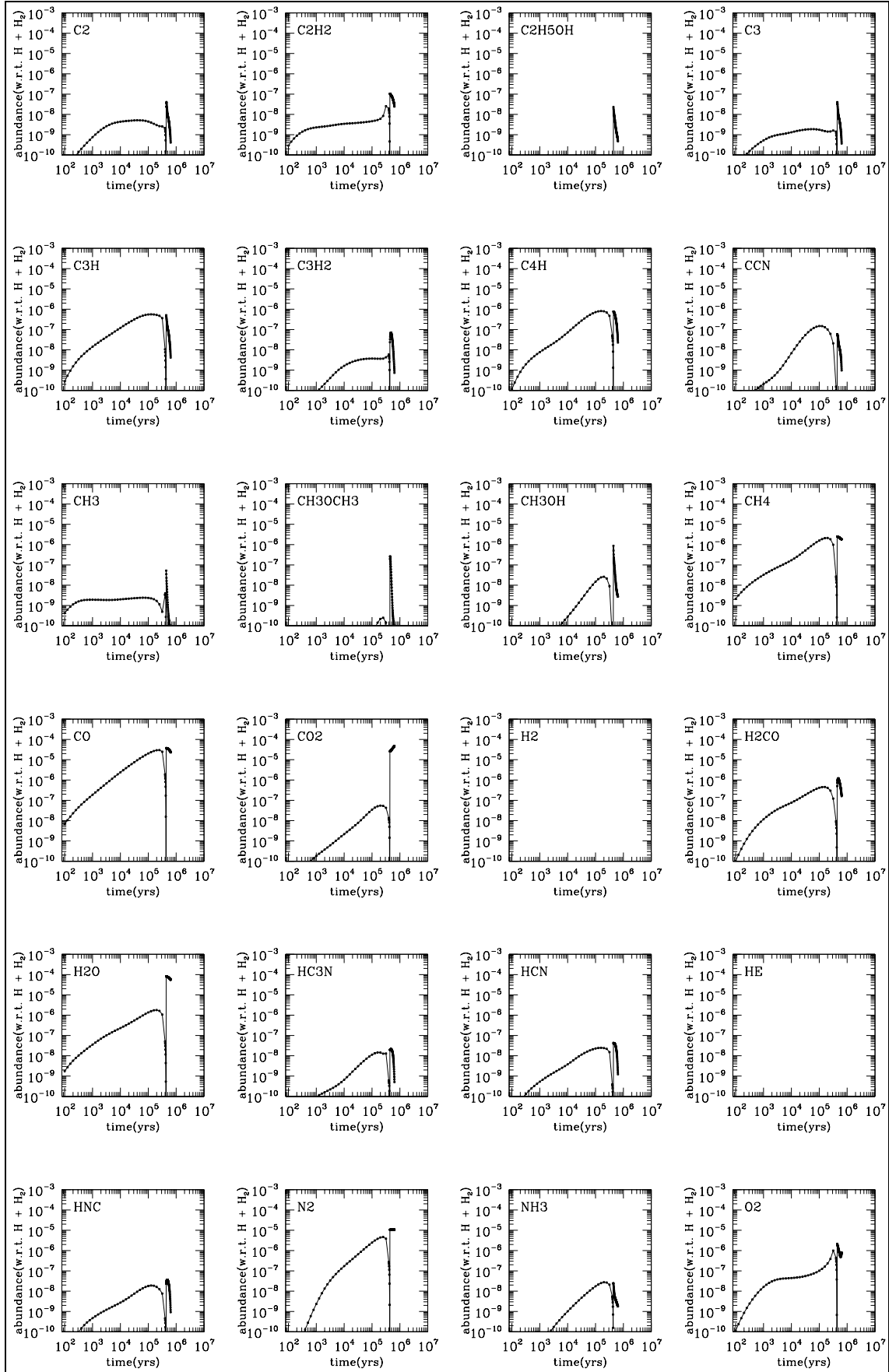


Fig. 7. Model 7 - Free fall collapse from $10,000 \text{ cm}^{-3}$ - H_2 starting abundance - gas phase data

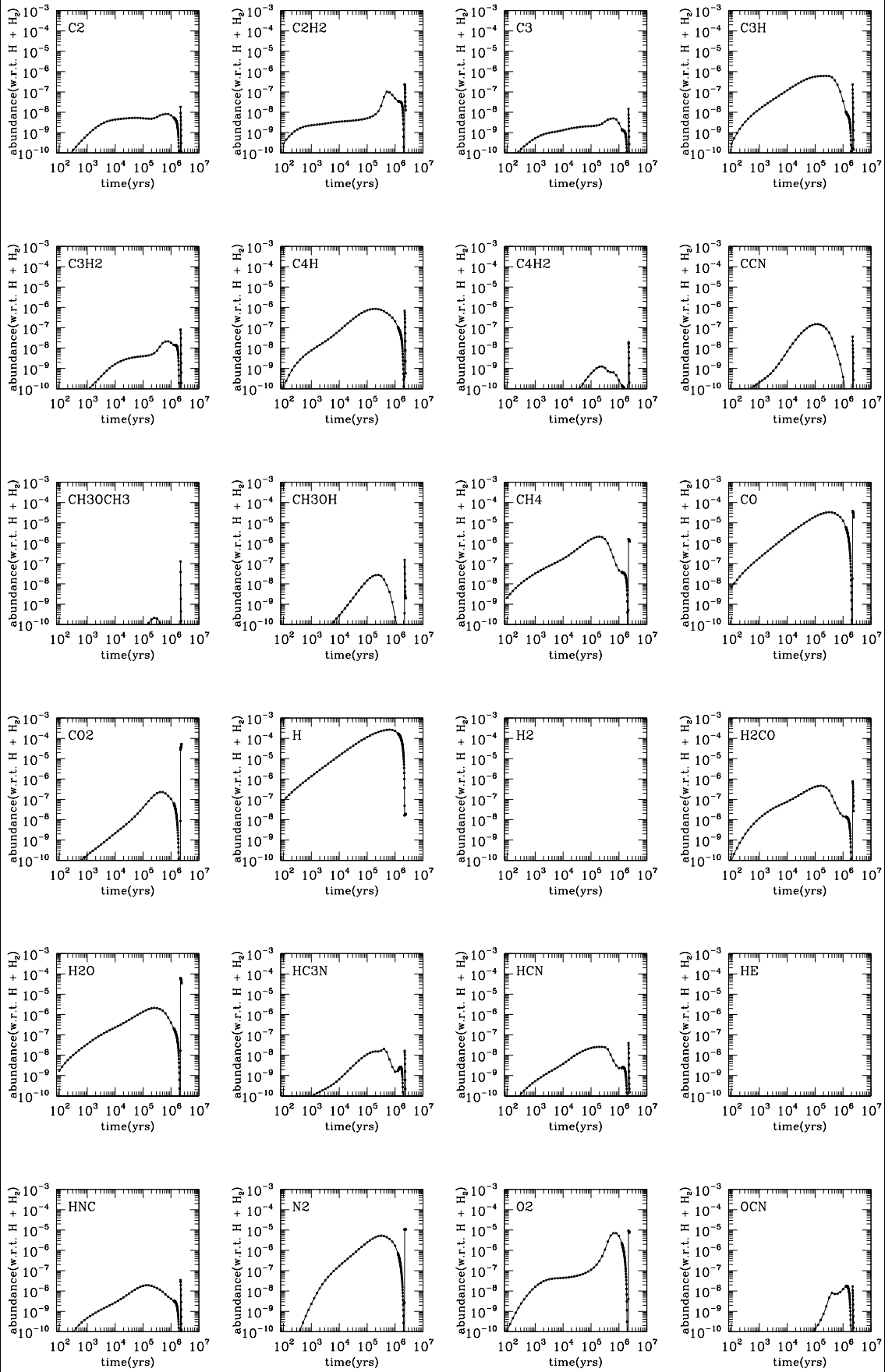


Fig. 8. Model 8 - Retarded collapse from $10,000\text{ cm}^{-3}$ - H_2 start-
ing abundance - gas phase data

References

- Aikawa Y. et al. 2008, *ApJ* 674, 993
- Allen M. & Robinson G.W. 1977, *ApJ* 212, 396
- Ball J.A. 1970, *ApJ* 162, L203
- Boogert A.C.A. et al. 1996, *A&A* 315, L377
- Boogert A.C.A. et al. 2008, *ApJ* 678, 985
- Bottinelli S., Ceccarelli C., Lefloch B., et al. 2004 *ApJ* 615, 354
- Bottinelli S., Ceccarelli C., Williams J. P. & Lefloch B. 2007 *A&A* 463, 601
- Breukers R.J.L.H. 1991, Ph.D. Thesis University of Leiden
- Brown P.D. 1988, Ph.D. Thesis University of Manchester
- Carral P. & Welch W.J. 1992, *ApJ* 385, 244
- Caselli P., Hasegawa T.I. & Herbst E. 1993, *ApJ* 408, 548
- Cazaux S., Tielens A.G.G.M., Ceccarelli C., et al. 2003, *ApJ* 593, L51
- Ceccarelli C., Loinard, L., Castets, A., Tielens, A.G.G.M., & Caux, E. 2000, *A&A* 357, L9
- Ceccarelli C. 2004. In *ASP Conf. Ser. 323: Star Formation in the Interstellar Medium*, 195, ed. Johnstone D., Adams F.C., Lin F.N.C, Neufeld D.A., & Ostriker E.C. Astronomical Society of the Pacific
- Charnley S.B., Tielens A.G.G.M. & Millar T.J. 1992, *ApJ* 399, L71
- Charnley S.B. et al. 1995, *ApJ* 448, 232
- De Pree C.G., Rodriguez L.F., Dickel H.R. & Goss W. M. 1995, *ApJ* 447, 220
- Draine B.T. 1978, *ApJS* 36, 595
- Duley W.W. & Williams D.A. 1984, *Interstellar Chemistry*, Academic Press.
- Dyson J.E. & Williams D.A. 1980, *Physics of the Interstellar Medium*, Manchester University Press
- Ehrenfreund P. & van Dishoeck E.F. 1998, *Advances in Space Research*, 21, 15-20.
- Ehrenfreund P. & Schutte W.A. 2000, *Advances in Space Research*, 25, 2177-2188.
- Fuente A., Neri R. & Caselli P. 2005, *A&A* 444, 481
- Garrod R.T. & Herbst E. 2006, *A&A* 457, 927
- Garrod R.T., Wakelam V. & Herbst E. 2007, *A&A* 467, 1103
- Garrod R.T., Widicus Weaver S.L. & Herbst E. 2008, *ApJ* 682, 283
- Garrod R.T., Vasyunin A.I., Semenov D.A., Wiebe D.S., Henning Th. 2009, *ApJ* 700, L43
- Gibb E. et al. 2000, *ApJ* 536, 347
- Grim R.J.A. & d'Hendecourt L.B. 1986, *A&A* 167, 161
- Hall P. 1997. In *Dust and Molecules in Evolved Stars*, 203, ed. Cherchneff I. & Millar T.J. Kluwer Academic Publishers
- Hasegawa T.I., Herbst E. & Leung C.M. 1992, *ApJS* 82, 167
- Hasegawa T.I. & Herbst E. 1993, *MNRAS* 261, 83
- Hassel G.E., Herbst E. & Garrod R.T. 2008, *ApJ* 681, 1385
- Herbst E. & Leung C.M. 1989, *ApJS* 69, 271
- Hindmarsh A.C. 1974, Lawrence Livermore Laboratory Rept. uclr-30001 Rev.3
- Hindmarsh A.C. 1983, In *Scientific Computing*, 55, ed. Stepleman R.S. et al. North-Holland Amsterdam
- Hollenbach D.J. & Salpeter E.E. 1971. *ApJ* 163, 155.
- Ikeda M. et al. 2001, *ApJ* 560, 792
- Ikeda M. et al. 2002, *ApJ* 571, 560
- Jørgensen J.K., Bourke T.L., Myers P.C., et al. 2005 *ApJ* 632, 973
- Lacy J.H., Faraji H., Sandford S.A. & Allamandola L.J. 1998, *ApJ* 501, L105
- Leung C.M., Herbst E. & Huebner W.F. 1984, *ApJS* 56, 231
- Maret S., Ceccarelli C., Caux E., et al. 2004, *A&A* 416, 577
- Maret S., Ceccarelli C., Tielens A.G.G.M., et al. 2005, *A&A* 442, 527
- Millar T.J. 1990, In *Molecular Astrophysics*, 115, ed. Hartquist T.W. University of Cambridge Press.
- Millar T.J. et al. 1991, *A&AS* 87, 585
- Millar T.J., Herbst E. & Charnley S.B. 1991, *ApJ* 369, 147
- Millar T.J., Farquhar P.R.A. & Willacy K. 1997, *A&AS* 121, 139
- Mumma M.J. et al. 1996, *Sci.* 272, 1310
- Öberg K.I. et al. 2008, *ApJ* 678, 1032
- Pontoppidan K.M. et al. 2008, *ApJ* 678, 1005
- Remijan A. et al. 2003, *ApJ* 590, 314
- Schutte W.A. & Greenberg J.M. 1988. In *Dust in the Universe*, 403. eds. Bailey M.E. & Williams D.A. Cambridge University Press.
- Shalabiea O.M. 1995. Ph.D. Thesis University of Leiden.
- Shalabiea O.M. & Greenberg J.M. 1995, *A&A* 303, 233
- Shu F. et al. 1993, In *Protostars and Planets III*, 3, eds. Levy E.H. & Lunine J.I. University of Arizona Press
- Snyder L. E. et al. 1974, *ApJ* 191, L79
- Spitzer L.J. 1978, *Physical Processes in the Interstellar Medium*, Wiley International
- Spitzer L.J. & Cochran W.D. 1973, *ApJ* 186, L23.
- Tapia M., Persi P. & Roth M. 1996, *A&A* 316, 102
- Tarafdar S.P. et al. 1985, *ApJ* 289, 220
- Tielens A.G.G.M. & Hagen W. 1982, *A&A* 114, 245
- Tielens A.G.G.M. & Allamandola L.J. 1987, In *Interstellar Processes*, 397, eds. Hollenbach D.J. & Thronson H.A. Dordrecht Kluwer
- Tielens A.G.G.M. & Charnley S.B. 1997, *Origins of Life and Evolution of the Biosphere*, 27, 34.
- van Dishoeck E.F. & Black J.C. 1986, *ApJS* 62, 109
- Völk et al. 1980, *A&A* 85, 316
- Wagenblast R. 1992, *MNRAS* 259, 155
- Whittet D.C.B. 1992, *Dust in the Galactic Environment*, Institute of Physics Publishing.
- Willacy K. 1993, Ph.D. Thesis University of Manchester
- Willacy K. & Millar T.J. 1998, *MNRAS* 298, 562
- Zuckerman B. et al. 1975, *ApJ* 196, L99